ORIGINAL ARTICLE

Inhibition of KDM5A attenuates cisplatin-induced hearing loss via regulation of the MAPK/AKT pathway

Chang Liu[1,2] · Zhiwei Zheng[1,2] · Wen Li[1,2] · Dongmei Tang[1,2] · Liping Zhao[1,2] · Yingzi He[1,2] · Huawei Li[1,2,3,4]

Abstract

The study aimed to investigate the potential role of lysine-specific demethylase 5A (KDM5A) in cisplatin-induced ototoxicity. The effect of the KDM5A inhibitor CPI-455 was assessed by apoptosis assay, immunofluorescence, flow cytometry, seahorse respirometry assay, and auditory brainstem response test. RNA sequencing, qRT-PCR, and CUT&Tag assays were used to explore the mechanism underlying CPI-455-induced protection. Our results demonstrated that the expression of KDM5A was increased in cisplatin-injured cochlear hair cells compared with controls. CPI-455 treatment markedly declined KDM5A and elevated H3K4 trimethylation levels in cisplatin-injured cochlear hair cells. Moreover, CPI-455 effectively prevented the death of hair cells and spiral ganglion neurons and increased the number of ribbon synapses in a cisplatin-induced ototoxicity mouse model both in vitro and in vivo. In HEI-OC1 cells, KDM5A knockdown reduced reactive oxygen species accumulation and improved mitochondrial membrane potential and oxidative phosphorylation under cisplatin-induced stress. Mechanistically, through transcriptomics and epigenomics analyses, a set of apoptosis-related genes, including *Sos1*, *Sos2*, and *Map3k3*, were regulated by CPI-455. Altogether, our findings indicate that inhibition of KDM5A may represent an effective epigenetic therapeutic target for preventing cisplatin-induced hearing loss.

Keywords KDM5A · Hair cells · Cisplatin · Ototoxicity · Apoptosis

Abbreviations

ABR	Auditory brainstem response
CP	Cisplatin
DEGs	Differentially expressed genes
GRPR	Gastrin-releasing peptide receptor
HCs	Hair cells
H&E	Hematoxylin and eosin
HIF-1	Hypoxia-inducible factor
IHCs	Inner hair cells
JmjC	Jumonji C
KDM5A	Lysine-specific demethylase 5A
KEGG	Kyoto Encyclopedia of Genes and Genomes
MMP	Mitochondrial membrane potential
OCRs	Oxygen consumption rates
OHCs	Outer hair cells
PI	Propidium iodide
ROS	Reactive oxygen species
SGNs	Spiral ganglion neurons
SOS	Son of sevenless
TUNEL	Terminal deoxynucleotidyl transferase-mediated dUTP nick-end-labeling

Chang Liu and Zhiwei Zheng contributed equally to this work.

✉ Yingzi He
yingzihe09611@126.com

✉ Huawei Li
hwli@shmu.edu.cn

1 Department of ENT Institute and Otorhinolaryngology, Eye and ENT Hospital, State Key Laboratory of Medical Neurobiology and MOE Frontiers Center for Brain Science, Fudan University, 83 Fenyang Road, Shanghai 200031, China

2 NHC Key Laboratory of Hearing Medicine, Fudan University, Shanghai 200031, People's Republic of China

3 Institutes of Biomedical Sciences, Fudan University, Shanghai 200032, People's Republic of China

4 The Institutes of Brain Science and the Collaborative Innovation Center for Brain Science, Fudan University, Shanghai 200032, People's Republic of China

Background

Cisplatin (CP) is a widely used agent for the treatment of various malignant cancers, including head and neck cancers, breast cancers, and lung cancers [1]. However,
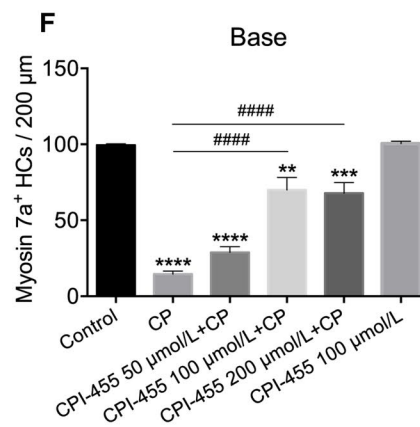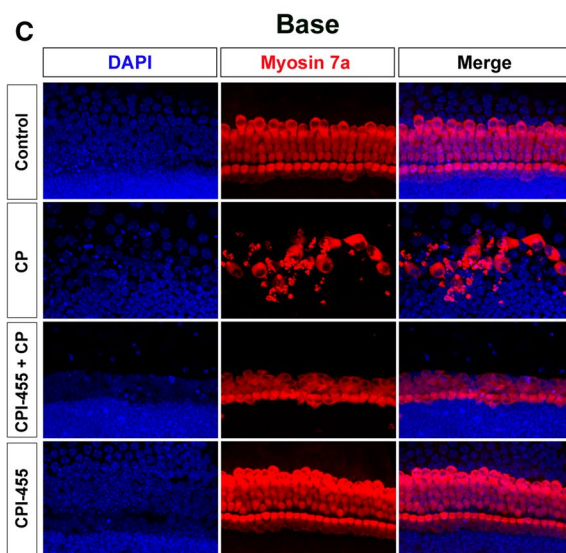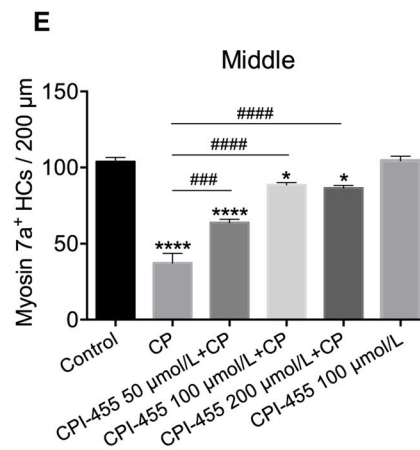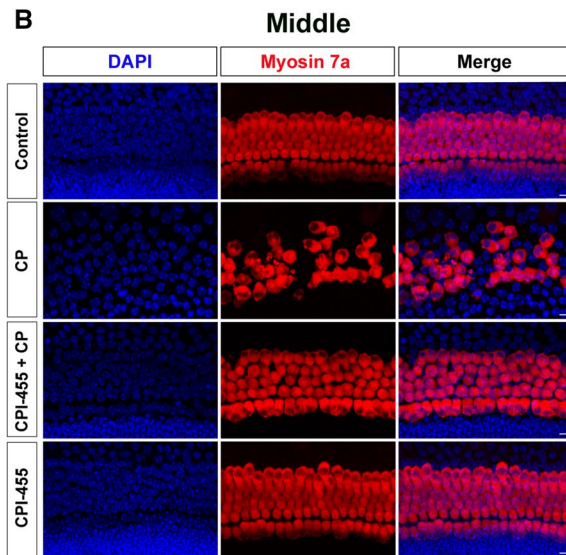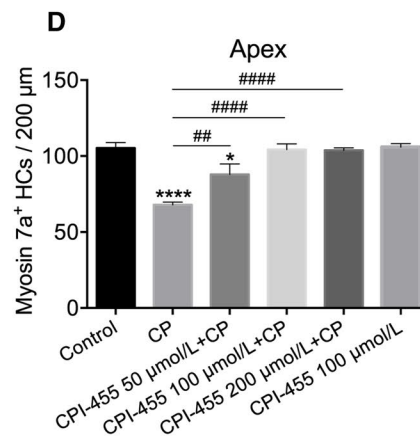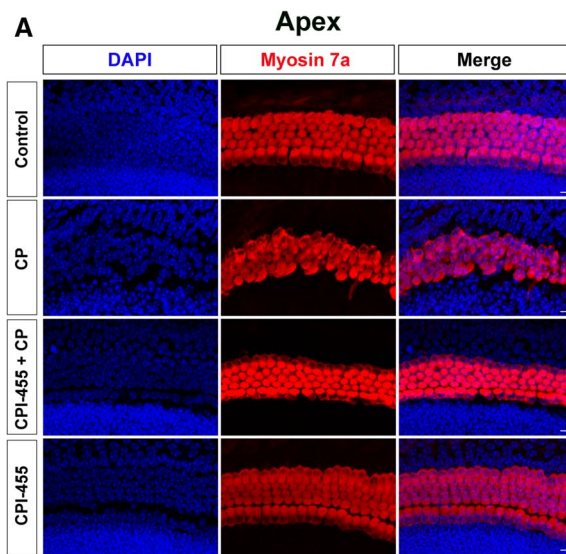
◄**Fig. 1** CPI-455 reduced CP-induced HC loss in ex vivo cochlear explants. **A–C** Cochlear explants were stained for Myosin 7a (red) and DAPI (blue). Scale bar 10 μm. **D–F** Graphical representation of the number of Myosin 7a–positive HCs per each treatment. The data are presented as the mean ± SEM values. *$P < 0.05$, **$P < 0.01$, ***$P < 0.001$, ****$P < 0.0001$ compared with the control; ##$P < 0.01$, ###$P < 0.001$, ####$P < 0.0001$ compared with CP only. The experiments were performed in triplicate. $n = 6$ cochleae for control group; $n = 6$ cochleae for CP group; $n = 6$ cochleae for 50 μmol/L CPI-455 + CP group; $n = 6$ cochleae for 100 μmol/L CPI-455 + CP group; $n = 6$ cochleae for 200 μmol/L CPI-455 + CP group; $n = 6$ cochleae for 100 μmol/L CPI-455 group

its application is seriously limited due to adverse effects [2, 3]. Ototoxicity is a severe side effect characterized by irreversible, progressive, and bilateral hearing loss [4]. Despite years of research, the underlying mechanism of CP-induced ototoxicity remains unclear, and little is known about the potential regulators in this process of ototoxicity.

Small molecules that interfere with protein–protein or protein–DNA interactions have offered a promising approach to controlling gene regulation. For example, gastrin-releasing peptide receptor (GRPR) acts as an inflammatory factor, and GRPR antagonists induce senescence and antiproliferative effects in several cancers [5]. Nickols et al. [6] revealed that targeting hypoxia-inducible factor (HIF-1)-DNA binding might be clinically relevant due to its complex role in cell survival and death pathways [7]. In addition, several studies focused on the development of novel treatment options [8], such as echinococcal infection [9] and chitosan–tripolyphosphate nanoparticles [10], as promising approaches in various cell lines. In recent years, the role of epigenetic modifications in the auditory field has received widespread attention [11–15].

Epigenetics refers to reversible and hereditary changes in gene function without altering the DNA sequence of the nucleus. Histone methylation is one of the most deeply studied post-translational modifications which regulate many biochemical processes [16]. As a member of the family of Jumonji C (JmjC) domain-containing histone demethylases, KDM5A regulates the demethylation of H3K4me3, an epigenetic mark associated with transcriptional activation [17]. Mounting evidence suggests that KDM5A plays an essential role in mitochondrial metabolism [18], cell cycle progression [19], cellular senescence [20], development and differentiation [21], and tumorigenesis [22]. However, the role of KDM5A in CP-induced ototoxicity is poorly understood. Here, we demonstrated that inhibiting KDM5A activity with CPI-455 reduces mitochondrial apoptosis, thus broadening our understanding of epigenetic modifications as novel targets to prevent CP-induced hearing loss.

Results

CPI-455 protects cochlear hair cells (HCs) against CP ototoxicity in vitro

First, we investigated whether CPI-455 could protect cochlear HCs against CP damage using ex vivo whole-organ cochlear explant cultures. According to our previous study [14], cochleae from P2 wild-type (WT) mice were dissected and pretreated with different CPI-455 concentrations (50, 100, and 200 μmol/L) for 2 h, followed by treatment with or without 30 μmol/L CP for 24 h. After 2 days of recovery in medium, cultured cochlear explants were immunolabelled with the HC marker myosin 7a. As shown in Fig. 1, compared with control group, HC loss in all three (base, middle, and apex) regions of the cochlea increased significantly after CP treatment. In contrast, treatment with CPI-455 remarkably attenuated the CP-induced HC loss. Of note, both inner HCs (IHCs) and outer HCs (OHCs) were found in intact arrangements in the CPI-455 + CP group (Fig. 1A–C). Quantitative results show that, compared to the CP group, 100 μmol/L of CPI-455 showed the most significant protective effect; therefore, 100 μmol/L was used as the optimal protective concentration of CPI-455 against CP-induced HC loss (Fig. 1D–F). Furthermore, the observation of the CPI-455-only group suggested no deleterious effects on the cochlear HCs treated with 100 μmol/L of CPI-455 alone (Fig. 1A–C). These results demonstrate that CPI-455 can prevent CP-induced cochlear HC death.

We further investigated the protective mechanisms of CPI-455 in cochlear HCs using the TUNEL assay. After exposure to CP, cochlear explants showed considerable TUNEL (red) signaling; on the contrary, the red fluorescence in CPI-455 + CP group decreased significantly compared with that of CP group (Fig. 2A–D), which indicated that CPI-455 suppressed CP-induced apoptosis in cochlear explants. Since the accumulation of reactive oxygen species (ROS) is related to CP-mediated HC apoptosis, MitoSOX™ red probe was used to detect the production of mitochondrial ROS. The results showed that cochlear explants exposed to CP displayed a significant increase in their fluorescence signal, indicating greater mitochondrial ROS generation than in the explants from the control group (Fig. 3A–D). In contrast, pretreatment of the cochlear explants with CPI-455 considerably ameliorated the CP-mediated overproduction of mitochondrial ROS (Fig. 3A–D).
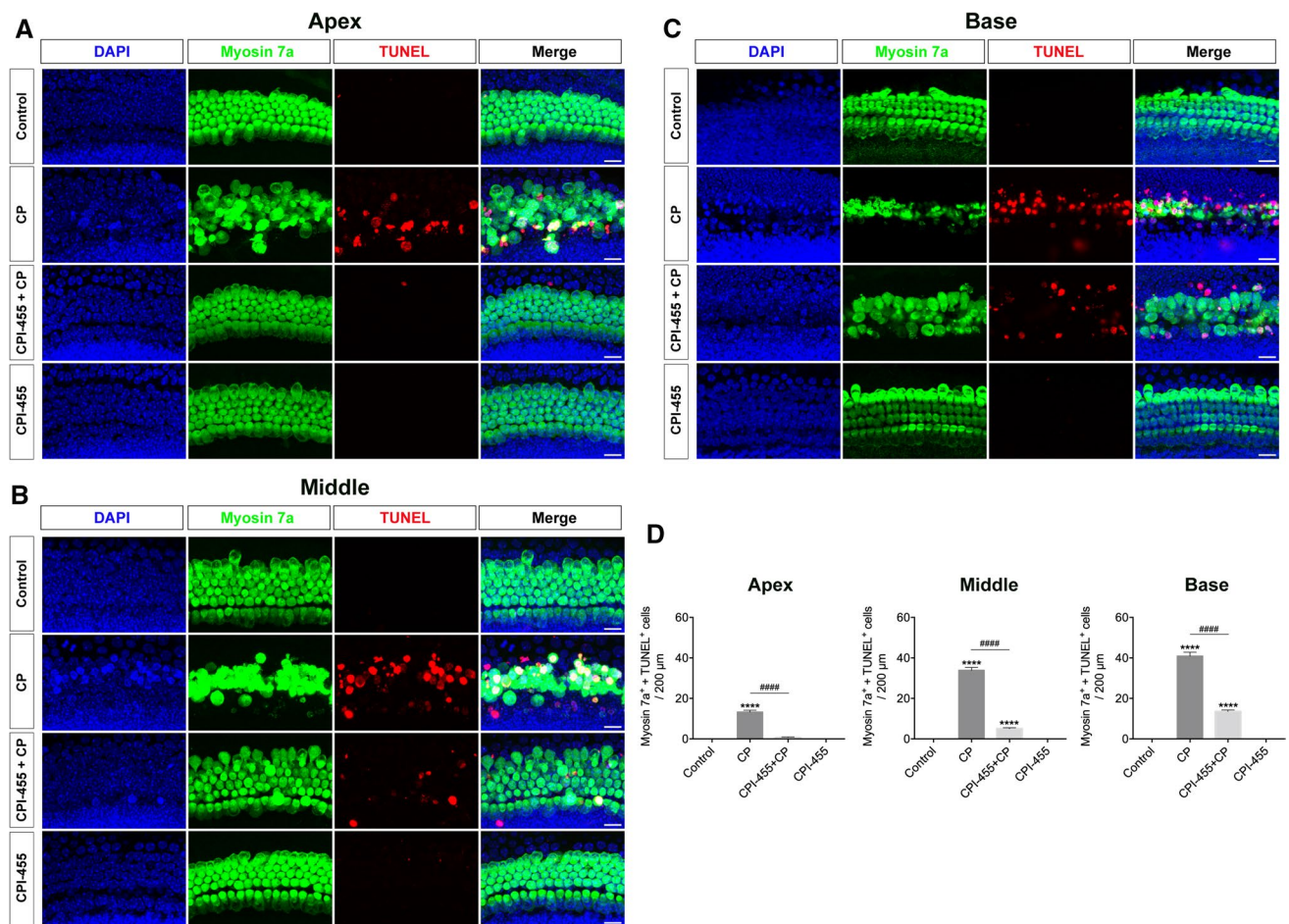
Fig. 2 CPI-455 reduced CP-induced HC apoptosis. **A–C** Cochlear explants were stained with Myosin 7a (green), TUNEL (red), and DAPI (blue). Images were captured from the cochlea's apex, middle, and base turns per condition. Scale bar 10 μm. **D** Statistical plot of Myosin 7a/TUNEL-positive cells in **A–C**. The data are presented as the mean ± SEM. ****$P < 0.0001$ compared with the control and ####$P < 0.0001$ compared with CP only. The experiments were performed in triplicate. $n = 8$ cochleae for control group; $n = 8$ cochleae for CP group; $n = 8$ cochleae for CPI-455 + CP group; $n = 8$ cochleae for CPI-455 group

CPI-455 protects cochlear spiral ganglion neurons (SGNs) against CP ototoxicity in vitro

Next, to study the effect of CPI-455 on SGNs, the cochlear SGNs of P2 mice were pretreated with a 100 μmol/L dose of CPI-455 for 2 h and then treated with or without 30 μmol/L of CP for 24 h. Figure 4A–C presents the typical confocal images of cochlear SGNs marked with Tuj-1. After CP treatment, the SGN morphological examination revealed that many nerve fibers were missing, and some blebs appeared on the remaining fibers. Compared with the untreated controls, the number of auditory nerve fibers decreased (Fig. 4D). Furthermore, the auditory nerve fiber bundles projecting from the SGNs to HCs were counted to quantify the effects of CP on the auditory nerve fibers. Neurites in the CP group were relatively shorter than those in the control group (Fig. 4E). In contrast, nerve fiber density and length were significantly increased in the CPI-455 + CP group compared with the CP-only group (Fig. 4D, E). These data suggest that CPI-455 can protect SGNs from CP-induced damage.

CPI-455 protects HCs and ribbon synapses from CP ototoxicity in vivo

To investigate the effect of CPI-455 in vivo, we used a previously reported CP injury model in vivo (Fig. 5A) [23]. After CP treatment, auditory brainstem response (ABR) showed that the hearing thresholds of the CP group were higher than that of the control group at all test frequencies. Treatment with a 0.5 mg/kg dose of CPI-455 did not significantly reduce the increase in the ABR threshold caused by CP. When the dose was increased to 2 mg/kg, however, it significantly reduced the auditory threshold shift (Fig. 5B). Immunofluorescence staining with anti–myosin 7a antibody showed that the number of HCs
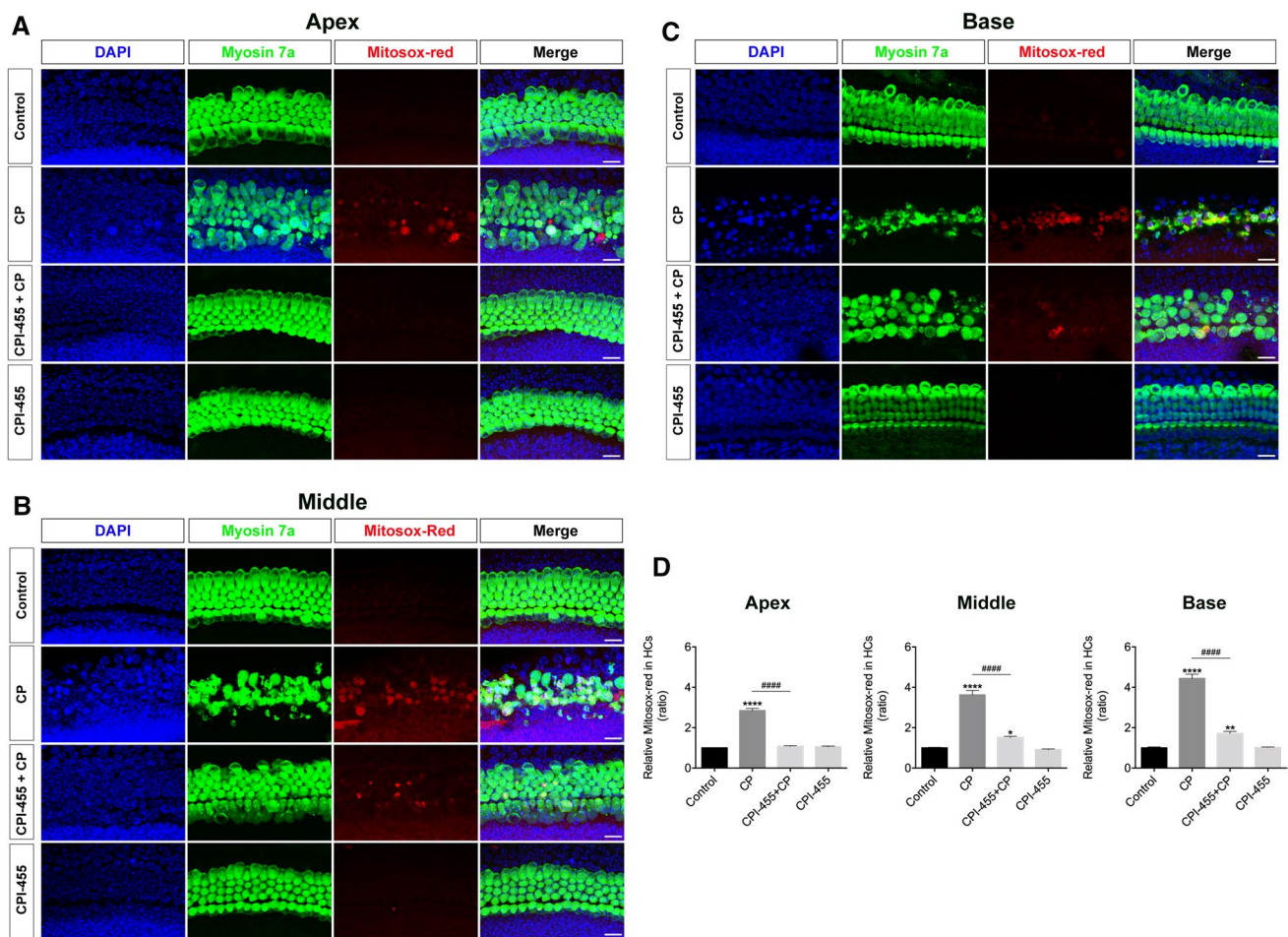
Fig. 3 CPI-455 reduced CP-induced ROS generation in cochlear HCs. **A–C** Cochlear explants were stained with Myosin 7a (green), MitoSOX™ red (red), and DAPI (blue). Images were captured from the cochlea's apex, middle, and base turns per condition. Scale bar 10 μm. **D** Comparison of MitoSOX™ red signals between each group. The data are presented as the mean ± SEM. *$P < 0.05$, **$P < 0.01$, ****$P < 0.0001$ compared with the control; ####$P < 0.0001$ compared with CP only. The experiments were performed in triplicate. $n = 9$ cochleae for control group; $n = 9$ cochleae for CP group; $n = 9$ cochleae for CPI-455 + CP group; $n = 9$ cochleae for CPI-455 group

in the apical, middle and basal cochlear regions decreased significantly after CP treatment compared with those of the control group (Fig. 5D–F). In contrast, CPI-455 treatment significantly increased the number of surviving HCs compared with that in the CP group (Fig. 5C). To better investigate the protective effect of CPI-455 on CP-induced hearing loss, we used a high-dose CP-induced ototoxicity model in C57BL/6J mice. C57BL/6J mice received a single intraperitoneal injection of 30 mg/kg of CP to induce hearing loss, and CPI-455 (10 mg/kg) was administered 2 h before CP administration. The ABR was tested 14 days after CP injection, and the results showed that treatment with CPI-455 protected against CP-induced hearing loss in the CP-induced ototoxicity model (Fig. S1 in Supporting Information). These data support the idea that CPI-455 has a significant protective effect on CP-induced hearing loss.

Ribbon synapses help to maintain normal hearing function and are vulnerable to ototoxic stimulation [24]. To investigate the effects of CPI-455 on the synapses, we identified the ribbon synapses of IHCs by double immunofluorescent labeling of presynaptic ribbons with anti-CtBP2 antibody (magenta) and postsynaptic ribbons with anti-GluR2 antibody (green). As demonstrated in Fig. 6A–C, after CP treatment, the numbers of ribbon synapses were significantly lower than those in the control group in all three regions examined. However, CPI-455 treatment remarkably lowered the CP-mediated loss of ribbon synapses (Fig. 6D, E). As the wave I amplitude reflects characteristic features of cochlear synaptopathy, we measured the average ABR wave I amplitude in different groups. As shown in Fig. 6F, CP administration decreased wave I amplitudes compared with those of the controls, whereas CPI-455 attenuated the
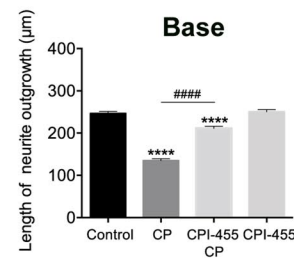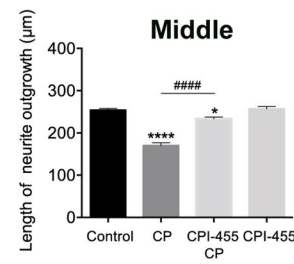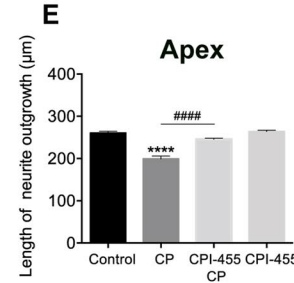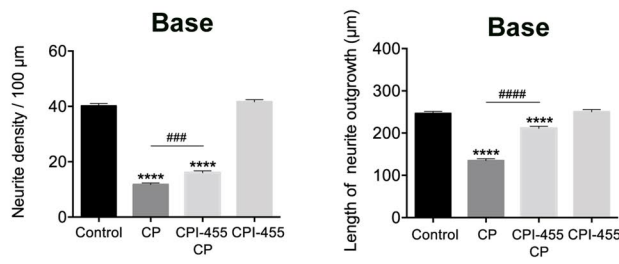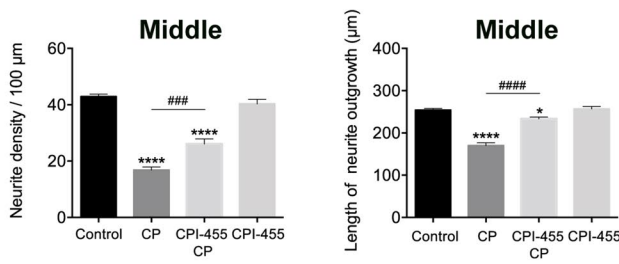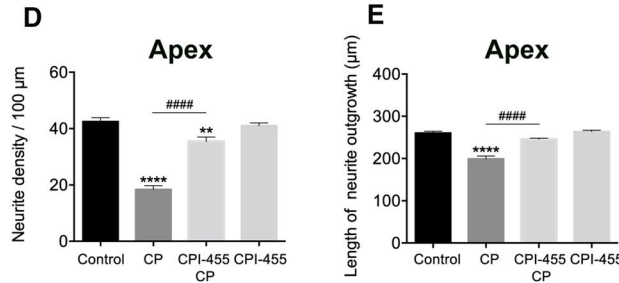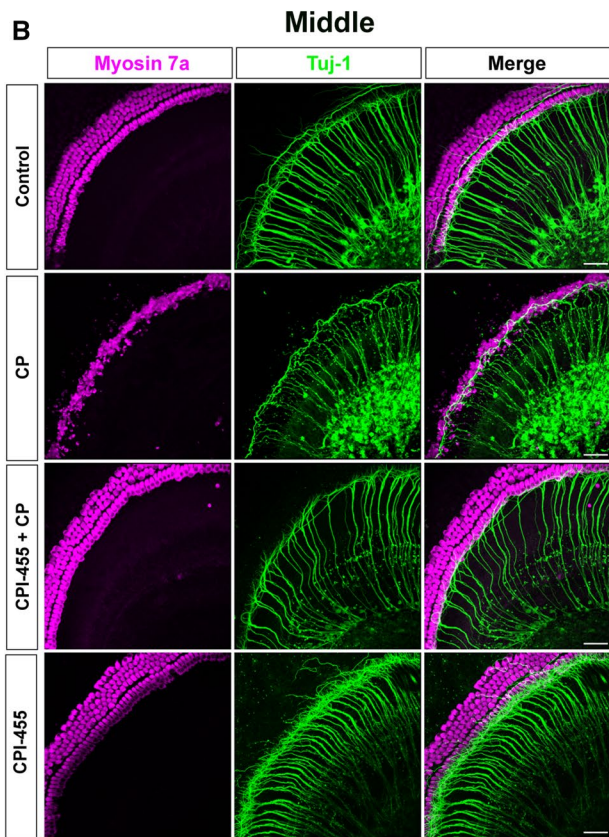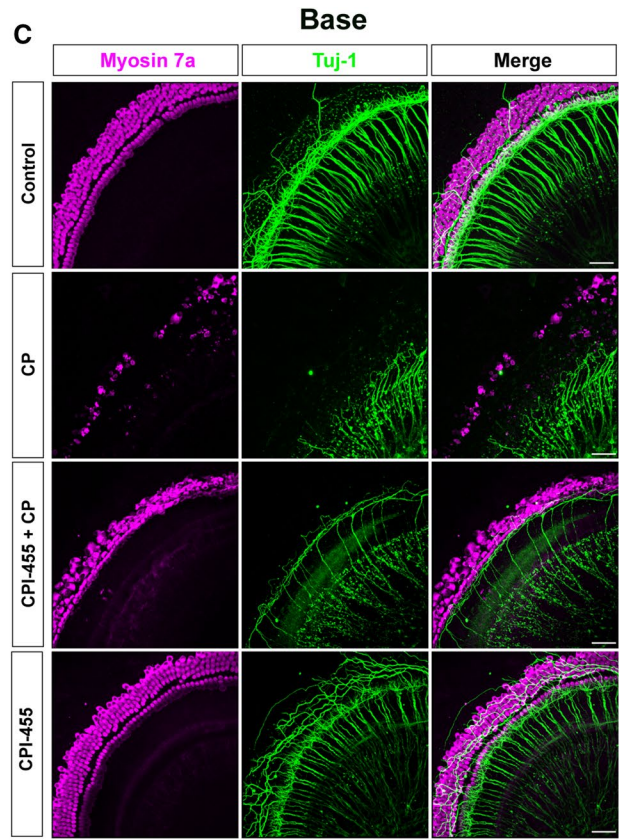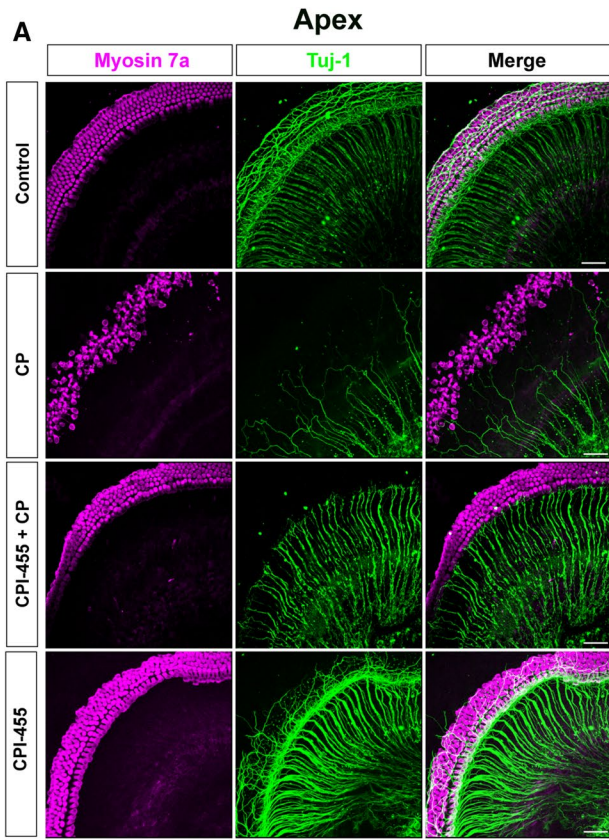
◄**Fig. 4** CPI-455 reduced CP-mediated SGNs loss in ex vivo cochlear explants. **A–C** Representative confocal photomicrographs show the spiral ganglion neurons from the apex, middle, and base turns of the cochlea treated with medium alone (control), CP-only (CP), CPI-455 + CP and CPI-455 only for 24 h and stained with Myosin 7a (magenta) and Tuj-1 (green). Scale bar 50 μm. **D**, **E** Quantification analysis of neurite densities and the length of neurite outgrowth from the apex, middle, and base turn of cochlear explants for all treatment conditions. The data are presented as the mean ± SEM. *$P < 0.05$, **$P < 0.01$, ****$P < 0.0001$ compared with the control; ###$P < 0.001$, ####$P < 0.0001$ compared with CP only. The experiments were performed in triplicate. $n = 10$ cochleae for control group; $n = 10$ cochleae for CP group; $n = 10$ cochleae for CPI-455 + CP group; $n = 10$ cochleae for CPI-455 group

CP-induced decrease. Therefore, these results demonstrate that the inhibition of KDM5A prolonged HC and ribbon synapse survival and rescued CP-induced hearing loss. To investigate any potential cytotoxicity of CPI-455 on normal tissues, we collected heart, liver, spleen, and lung tissue to analyze changes. Hematoxylin and eosin (H&E)-stained sections were visualized using a light microscope. No significant differences were found in these tissues between the control and CPI-455-only groups (Fig. S2 in Supporting Information), demonstrating that CPI-455 exhibits potent anti-apoptosis activity with insignificant toxicity in vivo. Two tumor cell lines were selected to test whether CPI-455 protects tumor cells during CP treatment, including Fadu (head and neck cancer) and HGC-27 (gastric cancer) cells. The results showed that both cell lines were sensitive to CP (Fig. S3A and D in Supporting Information). When treated with CPI-455, Fadu and HGC-27 cancer cells were sensitive at high doses (Fig. S3B and E in Supporting Information). When co-treated with CP and CPI-455, further reductions in cell survival were observed in both cell lines (Fig. S3C and F in Supporting Information). The results indicated that CPI-455 had no protective effects on these tumor cell lines. Instead, a synergistic effect with CP was observed on gastric cancer and head and neck cancer cell lines.

CPI-455 promotes the methylation level of H3K4 tri-methylation in the HCs under CP stress

Since CPI-455 is well known to inhibit the activity of the histone demethylase KDM5, the protein levels of KDM5A/B/C were detected by western blot analysis. The results showed that the KDM5A signal in the CP-exposed group was significantly higher than that of KDM5B and KDM5C compared to the control group (Fig. 7A, B). Consistent with the western blotting results, immunofluorescence analysis of cochlear HCs showed that CP treatment significantly upregulated KDM5A expression in the damaged HCs (Fig. 7C). Conversely, the use of CPI-455 decreased the KDM5A level in the survival HCs under CP treatment (Fig. 7A–C). Furthermore, the overall H3K4me3 levels declined in the CP

group compared with the untreated control group, while the CPI-455 treatment increased the overall level of H3K4me3 in the HCs (Fig. 7A–D). The results suggest that CPI-455 may attenuate CP-mediated HC apoptosis via KDM5A inhibition.

Knockdown of KDM5A attenuates ROS signaling-mediated apoptosis in HEI-OC1 cells

To test the above finding, we knocked down KDM5A in HEI-OC1 cells by small interfering RNA (siRNA) transfection. The transfection efficiency of siRNA-KDM5A was confirmed using qRT-PCR (Fig. S4A in Supporting Information) and western blot (Supporting Information Fig. S4B–C) assays. At 48 h after siRNA transfection, the HEI-OC1 cells were treated with 30 μmol/L of CP for 24 h. Annexin V-FITC and PI assays were carried out to detect the percentages of early apoptotic cells (Annexin V-FITC positive, PI negative) and late apoptotic cells (Annexin V-FITC/PI double positive) (Fig. 8A). We found that, after 24 h of culture without CP treatment, KDM5A inhibition itself had almost no effect on early (bottom right quadrants) and late apoptosis (top right quadrants). With CP treatment, the proportions of early and late apoptotic cells in the siRNA-KDM5A group were reduced compared with those in the CP-only group (Fig. 8B, C), suggesting that knockdown of KDM5A significantly suppressed CP-induced HEI-OC1 cell apoptosis.

Multiple studies have demonstrated that ROS is the main cause of HC death induced by ototoxic drugs [25]. To investigate whether inhibiting KDM5A protects HCs against CP-induced damage by reducing the production of ROS, we used CellROX™ green, a fluorescent probe that emits green fluorescence once oxidized by ROS, to measure the total ROS level in HEI-OC1 cells. The results showed that, after CP exposure, the levels of ROS increased significantly, while the downregulation of KDM5A could reduce the production of ROS. Flow cytometry data confirmed that HEI-OC1 cells in the CP + siRNA-KDM5A group produced significantly lower ROS than those in the CP group (Fig. 8D–F). Given that mitochondrial disorders can lead to ROS accumulation [26], we next sought to find out whether an improvement in mitochondrial function accompanied the anti-apoptosis effect of KDM5A inhibition. Changes in mitochondrial membrane potential (MMP) were investigated using Rhodamine 123 probe. As shown in Fig. 8G, MMP levels decreased significantly after 24 h of CP exposure compared to the control group, indicating that CP had an impairing effect on mitochondrial function. In contrast, knockdown of KDM5A alleviated the decline of MMP, revealing a protective role of CPI-455 in mitochondria (Fig. 8H, I). Next, we further investigated the effect of si-KDM5A on mitochondrial respiratory capacity. Oxygen
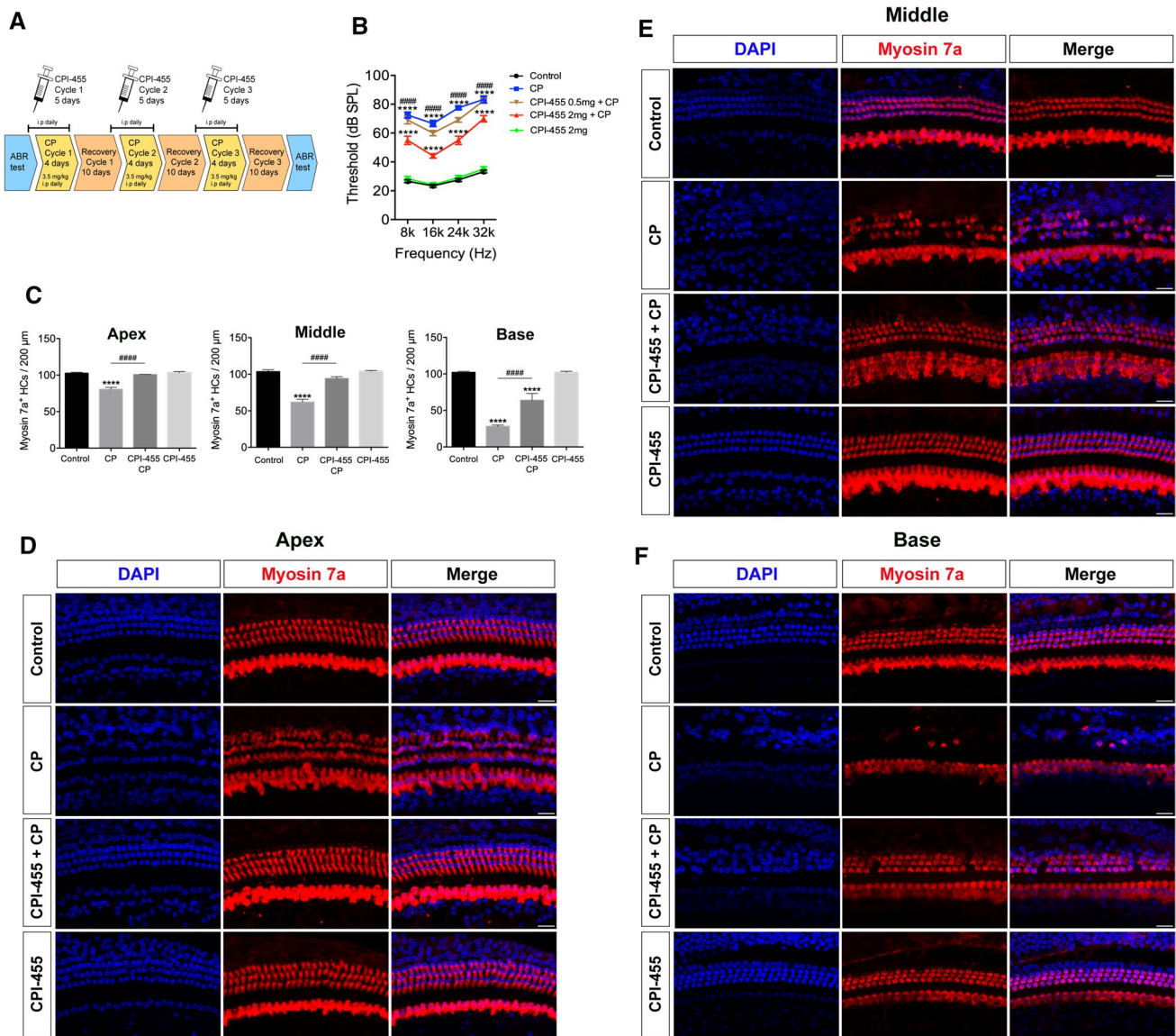
Fig. 5 CPI-455 protected against CP-induced hearing loss in vivo. **A** Experimental workflow. **B** ABR analysis. Data are shown as mean ± SEM values. ****$P < 0.0001$ compared with the control; ####$P < 0.0001$ compared with CP only. $n = 6$ mice for each group. **C** Graphical representation of the number of Myosin 7a–positive HCs. Data are shown as mean ± SEM values. ****$P < 0.0001$ com-

pared with the control; ####$P < 0.0001$ compared with CP only. The experiments were performed in triplicate. $n = 10$ cochleae for control group; $n = 10$ cochleae for CP group; $n = 10$ cochleae for CPI-455 + CP group; $n = 10$ cochleae for CPI-455 group. **D–F** Cochleae were stained with Myosin 7a (red) and DAPI (blue). Scale bar 10 μm

consumption rates (OCRs), an index of mitochondrial respiratory capacity, were measured in HEI-OC1 cells using a Seahorse XF Cell Mito Stress Test (Fig. 8J). Following CP treatment of HEI-OC1 cells for 24 h, basal OCR, adenosine triphosphate production, and maximum and spare respiration were significantly reduced; KDM5A knockdown partially prevented these changes (Fig. 8K–N). These results confirmed that KDM5A inhibition could attenuate CP-induced mitochondrial dysfunction in HEI-OC1 cells.

CPI-455 reduces CP-induced ototoxicity through regulating MAPK and PI3K/AKT signaling

To identify potential transcription factors regulated by CPI-455 in HEI-OC1 cells during CP-induced injury, we utilized RNA sequencing (RNA-Seq). According to the results of the RNA-Seq, 3264 were significantly downregulated, and 3318 were upregulated by CPI-455 + CP (vs. CP). Gene expression patterns were presented as a volcano map (Fig. 9A).

Fig. 6 CPI-455 protected mice from CP-induced synapses loss. **A–C** Cochleae were stained for CtBP2 (magenta) and GluR2 (green). Scale bar 10 μm. **D**, **E** Quantification of CtBP2-immunolabeled or GluR2-immunolabeled synaptic ribbons per IHCs. The data are presented as the mean ± SEM values. *$P < 0.05$, ***$P < 0.001$, ****$P < 0.0001$ compared with the control; ####$P < 0.0001$ compared with CP only. The experiments were performed in triplicate. $n = 6$ cochleae for control group; $n = 6$ cochleae for CP group; $n = 6$ cochleae for CPI-455 + CP group; $n = 6$ cochleae for CPI-455 group. **F** ABR wave I amplitudes analysis. Data are shown as mean ± SEM values. ****$P < 0.0001$ compared with the control; ####$P < 0.0001$ compared with CP only. $n = 6$ mice for each group
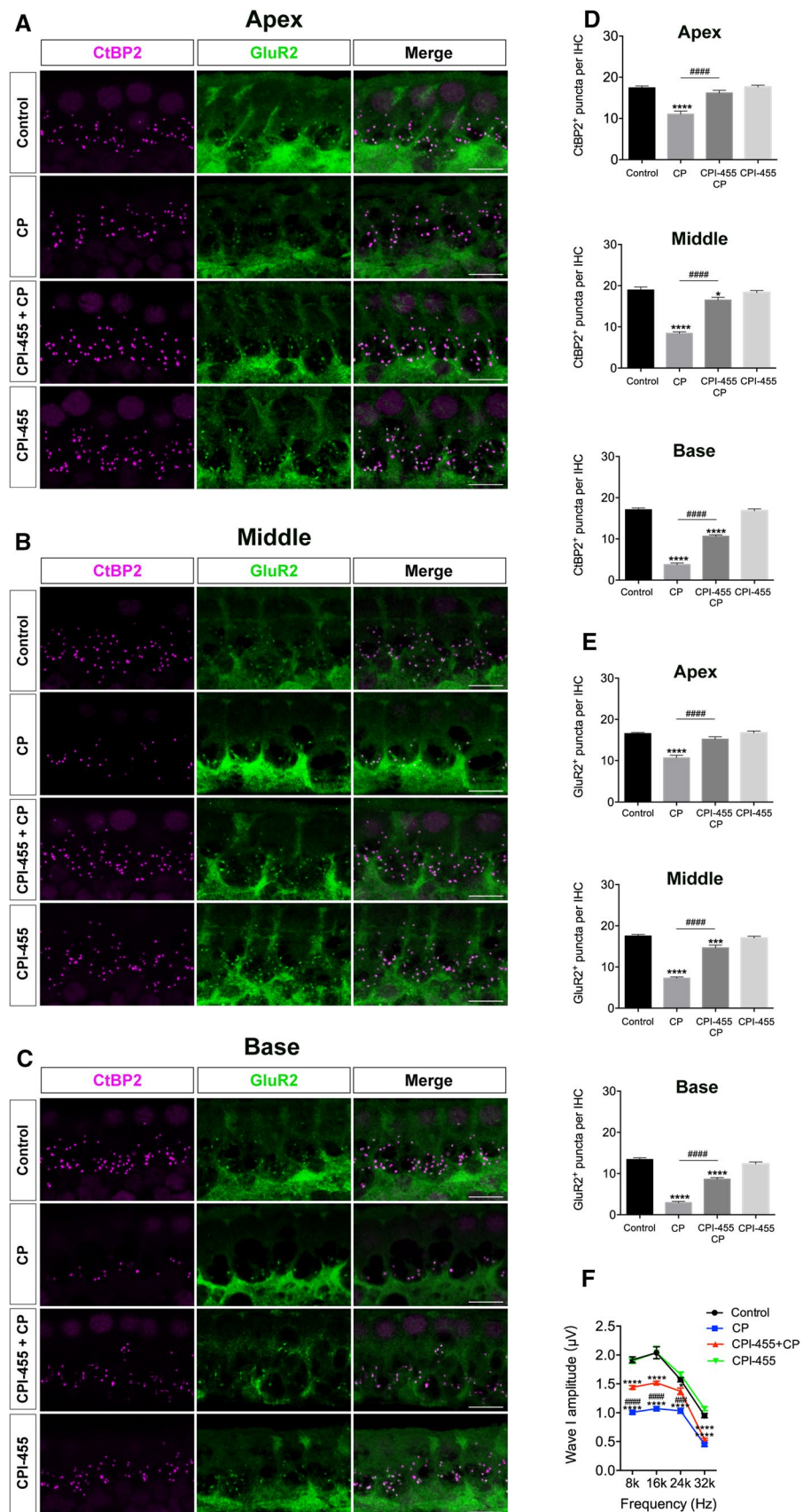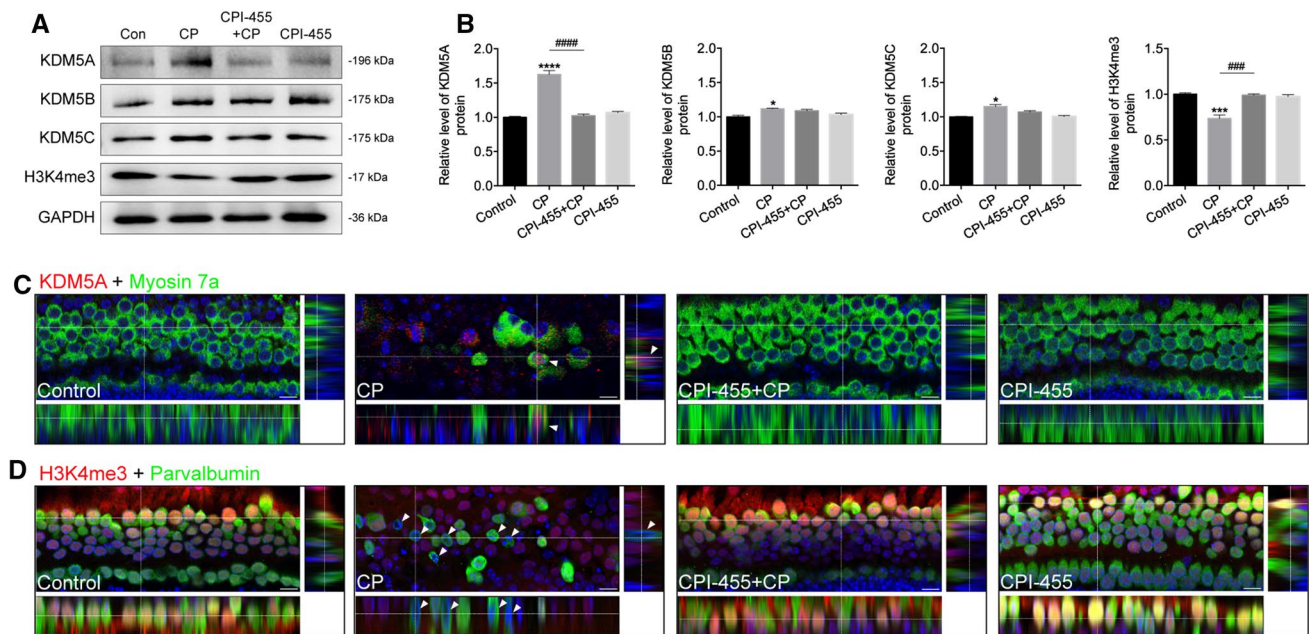
Fig. 7 CPI-455 affected KDM5A and H3K4me3 expression in cochlear HCs. **A**, **B** The protein levels of KDM5A, KDM5B, KDM5C, and H3K4me3. GAPDH served as an internal control. Data are presented as mean ± SEM values. $*P < 0.05$, $***P < 0.001$, $****P < 0.0001$ compared with the control; $^{###}P < 0.001$, $^{####}P < 0.0001$ compared with CP only. The experiments were performed in triplicate. **C** Cochleae were stained for KDM5A (red) and Myosin 7a (green). **D** Cochleae were stained for H3K4me3 (red) and parvalbumin (green). Images were captured from the middle turns of the cochlea. Scale bars 10 μm

Kyoto Encyclopedia of Genes and Genomes (KEGG) pathway enrichment analysis was conducted, and the top pathways of the enrichment analysis are shown in Fig. 9B. To verify the differentially expressed genes (DEGs), we selected some genes and detected them by qRT-PCR (Online Table 1 and Fig. 9C). Given that H3K4me3 is commonly defined as an activating histone modification and that CPI-455 produces a marked global increase in H3K4 methylation, we hypothesized that CPI-455 might promote an increase in CP-induced silent gene expression by increasing H3K4me3 levels in specific gene promoter regions. To test this, we performed CUT&Tag coupled with quantitative PCR (qPCR) assay on HEI-OC1 cells. Compared to the CP group, we observed a substantial increase in H3K4me3 within the promoters of the SOS family members *Sos1* and *Sos2* and the MAPK key regulator *Map3k3* in cells treated with both CP and CPI-455 (Fig. 9D–F). The data suggest that CPI-455 mediates the increase in H3K4me3 promoter occupancy, which may enhance the expression of a group of apoptosis-related genes.

Western blot assay was performed to verify the expression of several critical factors of the MAPK and PI3K/AKT signaling pathway and apoptosis-related proteins in each group. The expression of the pro-apoptotic proteins, including p-P38, p-JNK, BAX, and cleaved caspase-3, was significantly higher in the CP group compared to the control group (Fig. 9G). In contrast, the expression levels of anti-apoptotic proteins, including p-AKT, p-PI3K, and Bcl-2, were decreased in the CP group compared to the control group (Fig. 9G). After CPI-455 treatment, the expression of both pro-apoptotic and anti-apoptotic proteins was similar to that of the control group (Fig. 9H). Together, these results show that CPI-455 treatment might protect against CP-induced cell death by regulating MAPK and PI3K/AKT signaling.

Discussion

Various studies show that epigenetics, such as histone modification, is closely related to inner ear development and hearing loss caused by multiple factors, so epigenetic modification may be a new therapeutic strategy [11, 12, 14]. Our previous research indicated that the expression level of LSD1 (KDM1A) in injured HCs and SGNs increases significantly after CP or neomycin damage. We also found that LSD1 by small compounds effectively inhibited apoptosis and promoted the survival of HCs and SGNs [11, 12]. These results suggested that histone methylated modification is closely involved in the auditory system. In the follow-up study on the role of crucial histone demethylases conducive to the survival of HCs, we found that KDM5A was correlated with the survival of HCs after CP-induced injury.
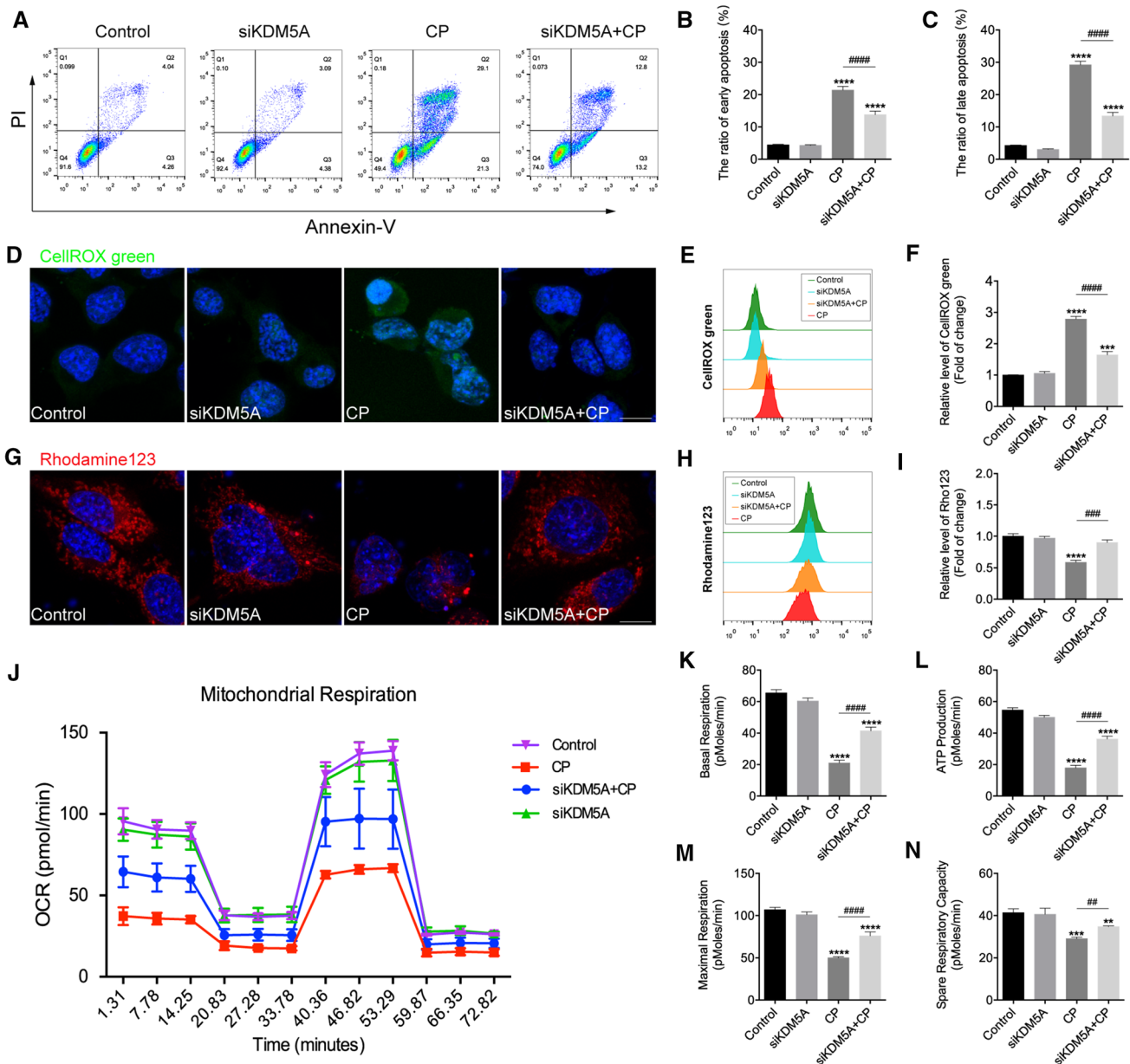
**Fig. 8** Downregulation of KDM5A reduced CP-induced apoptosis in HEI-OC1 cells. **A–C** Effects of KDM5A on early (Annexin V-FITC positive, PI negative) and late (Annexin V-FITC/PI double positive) cell apoptosis were (**A**) determined via flow cytometry and (**B**, **C**) quantified. The data are presented as three independent experiments' mean ± SEM values. $****P < 0.0001$ compared with the control; $####P < 0.0001$ compared with CP only. **D–F** Representative images and histogram analysis of CellROX™ green in HEI-OC1 cells. Scale bar = 10 μm. The data are presented as three independent experiments' mean ± SEM values. $***P < 0.001$, $****P < 0.0001$ compared with the control; $####P < 0.0001$ compared with CP only. **G–I** Representative images and histogram analysis of Rhodamine 123 in HEI-OC1 cells. Scale bar 10 μm. The data are presented as three independent experiments' mean ± SEM values. $****P < 0.0001$ compared with the control; $###P < 0.001$ compared with CP only. **J–N** OCRs and bioenergetics parameters in HEI-OC1 cells from each group. The data are presented as mean ± SEM values. $**P < 0.01$, $***P < 0.001$, $****P < 0.0001$ compared with the control; $##P < 0.01$, $####P < 0.0001$ compared with CP only. The experiments were performed in triplicate

A growing pool of literature demonstrates that KDM5A is highly expressed in various cancer tissues, including gastric cancer, acute myeloid leukemia, and breast cancer, and proves that KDM5A is a potential molecular biomarker and novel target for cancer therapy [27–29]. In cancer treatment, KDM5A-specific inhibitors can reduce the drug resistance of cancer cells and induce tumor cell death [27, 30, 31]. KDM5A is an essential epigenetic factor that maintains neural progenitor cells in an undifferentiated state by inhibiting astrocyte differentiation [32]. Interestingly, a recent study
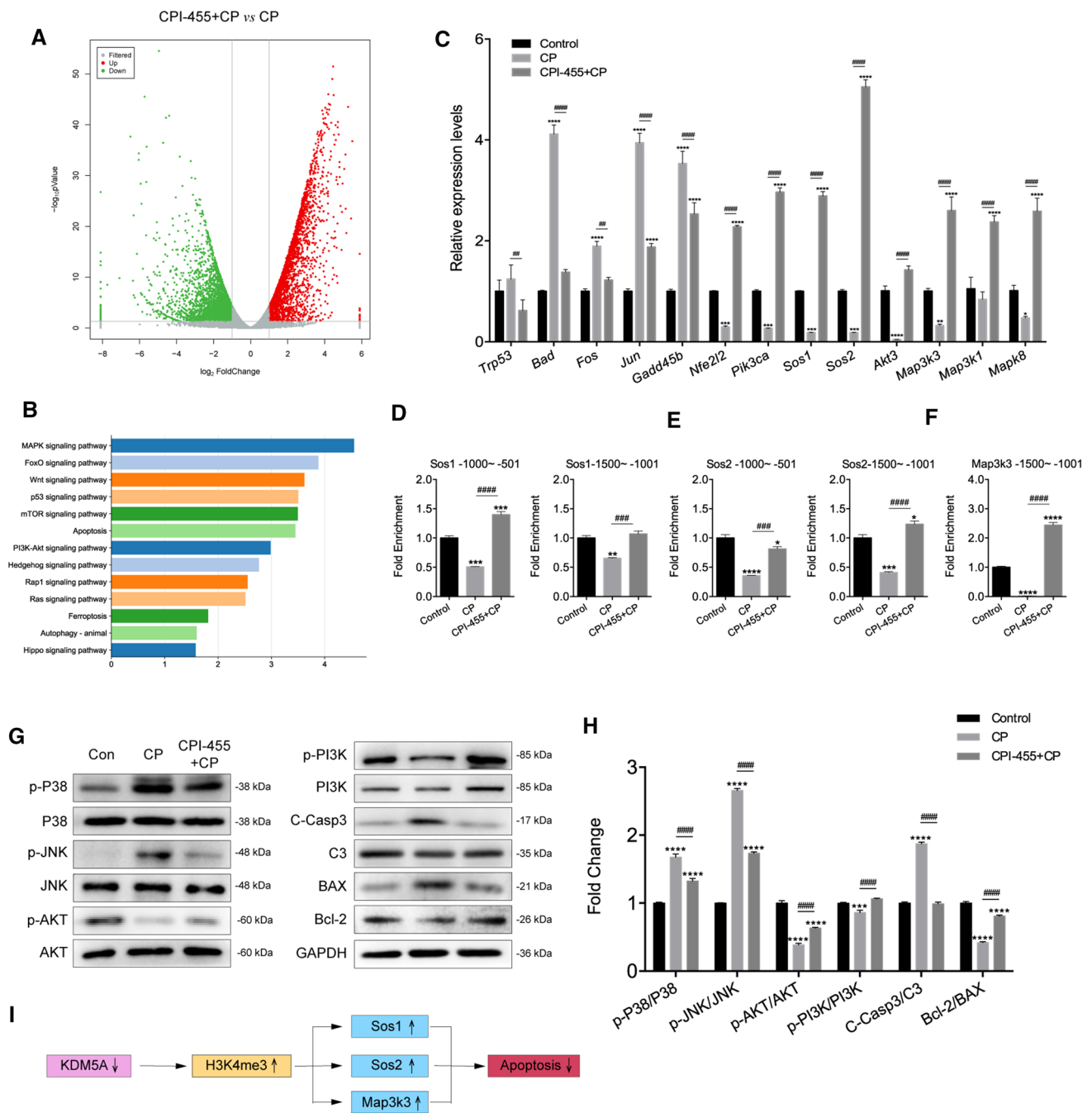
Fig. 9 CPI-455 reduced CP-induced HC death via multiple signaling pathways. **A** Volcano plot representing gene-expression differences between CPI-455+CP and CP. **B** KEGG analysis showed the distribution of terms exhibiting statistically significant differences. **C** The differentially expressed genes were verified in HEI-OC1 cells by qRT-PCR. Data are presented as mean±SEM values. *$P < 0.05$, **$P < 0.01$, ***$P < 0.001$, ****$P < 0.0001$ compared with the control; ##$P < 0.01$, ####$P < 0.0001$ compared with CP only. **D–F** Enrichment of H3K4me3 on promoters of *Sos1*, *Sos2*, and *Map3k3* genes. Data were normalized to the IgG controls. Data are pre-sented as mean±SEM values. *$P < 0.05$, **$P < 0.01$, ***$P < 0.001$, ****$P < 0.0001$ compared with the control; ###$P < 0.001$, ####$P < 0.0001$ compared with CP only. **G, H** The protein levels of p-P38, P38, p-JNK, JNK, p-AKT, AKT, p-PI3K, PI3K, C-Casp3, C3, BAX, and Bcl-2 in HEI-OC1 cells. GAPDH serves as an internal control. Data are presented as mean±SEM values. ***$P < 0.001$, ****$P < 0.0001$ compared with the control; ####$P < 0.0001$ compared with CP only. The experiments were performed in triplicate. **I** Summary of the working thesis of the study

revealed that the inhibition of KDM5A can improve the protective effect of dexmedetomidine on renal failure [33]. Therefore, KDM5A seems to regulate cell survival through different mechanisms in a context-dependent manner. However, the detailed involvement of KDM5A in ototoxic diseases has rarely been studied.

In this study, we employed a mouse model to explore the role of KDM5A in CP-induced ototoxicity. The results of western blot and immunofluorescence showed that the expression of KDM5A was upregulated in the CP injury group. However, because the proteins used for Western blot analysis were isolated from the entire cochlear epithelium, and immunofluorescence staining focused on the expression of KDM5A in the hair cell layer, the immunostaining of KDM5A could not fully reflect the changes detected by Western blot. CPI-455 was designed as a cell-permeable prodrug, which can change the level of H3K4me3, thus laying the foundation for the further development of therapeutic drugs against KDM5 potential [34]. By employing mouse in vitro and in vivo CP injury models, we found that the inhibition of KDM5A histone lysine demethylase with CPI-455 protected against CP-induced hearing loss. C57BL/6J mice have been widely used as an optimal mouse model for the study of age-related hearing loss. These mice maintain normal hearing for 13 weeks, then display the classic pattern of age-related hearing loss, i.e., high-frequency hearing loss, beginning around 13–26 weeks of age, and the loss progresses toward the low frequency [35–39]. Hearing loss was reported at all frequencies up to 65 weeks, with no measurable hearing response at 78 weeks [40]. Previous studies have shown that loss of ribbon synapses is the initial pathological event in the early aging stage [41, 42]. Xiong et al. showed that younger C57BL/6J mice (< 4 months) had an average number of HCs, SGNs, and synapses; however, for mice aged 4 months, the number of cochlear ribbon synapses was reduced in the high-frequency cochlear regions, and significant elevations in the hearing threshold initially appeared at a high frequency at 4 months and across frequencies at 6 months, which suggests that the lifespan of 4 months was the early stage of aging [41]. In our in vivo experiment, to be consistent with the in vitro data, C57BL/6J mice were used and treated with CP using a three-cycle regimen. At the time of analysis, the mice were 14–15 weeks (< 3.5 months) old. Although this mouse model was < 4 months old, with normal hearing and an average number of HCs and synapses, to illustrate better the protective effect of CPI-455 on CP-induced hearing loss and exclude the influence of age-related hearing loss factors, we used a C57BL/6J mouse ototoxicity model with a high dose of CP. Our result showed that the administration of CP at 30 mg/kg caused significant elevations in the hearing threshold, and CPI-455 treatment protected against CP-induced hearing loss in this mouse model. Taken together, these data supported the idea that CPI-455

could be used as a candidate therapeutic agent for protection against CP-induced ototoxicity.

Oxidative damage would impair mitochondrial function and cause cell death. In this study, we showed that knockdown of KDM5A reduced CP-induced production of ROS and disruption of MMP in HCs, suggesting that KDM5A inhibition might achieve its otoprotective effect by inhibiting the generation of ROS and maintaining the integrity of mitochondria. As an indicator of mitochondrial function, the dysfunction of MMP might lead to a proton gradient within the inner mitochondrial membrane. In a healthy mitochondrion, the net negative charge is majorly generated by cytochrome c. However, when the mitochondrial function is impaired by ototoxic disease, the consequences are mitochondrial membrane permeabilization and cytochrome c release into the cytosol, causing an immediate dissipation of $\Delta\psi m$. It is speculated that the destruction of MMP may inhibit the respiratory capacity of mitochondria. Previous studies have shown that the loss of KDM5A could increase mitochondrial respiration, thus restoring the differentiation of mouse embryonic fibroblasts, suggesting that KDM5A may be an epigenetic regulator that controls metabolic processes and synchronizes energy homeostasis with differentiation signals [18]. Our study examined whether knockdown of KDM5A could improve the impaired OXPHOS activity in HEI-OC1 under CP treatment. As shown in Fig. 8J, our results indicate that KDM5A knockdown significantly increases mitochondrial OCRs, suggesting that KDM5A inhibition may be a potential approach to prevent ototoxicity.

Although KDM5A inhibition restored mitochondrial function by reducing mitochondrial ROS generation and recovering CP-treated cells' respiratory ability, the potential mechanisms were not fully elucidated. To determine the potential target of KDM5A inhibition for protection, we performed RNA-Seq analysis in HEI-OC1 cells. Of the crucial enriched pathways, PI3K/AKT and Ras/MAPK, the ROS-sensitive regulators, are two significant mediators of CPI-455 for HC protection. The PI3K/AKT signal pathway has been shown to regulate diverse cellular functions in different systems, including apoptosis, proliferation, and metabolism [43]. Many studies have demonstrated that the PI3K/AKT pathway is a crucial signaling pathway in regulating HC development, apoptosis, and the proliferation of otic progenitors [44]. The PI3K/AKT pathway participates in the survival and protection of auditory HCs by inhibiting pro-apoptotic signals and mitochondria-produced ROS [45, 46]. Zhang et al. demonstrated that superoxide dismutase 2 overexpression counteracted the noise and kanamycin-induced hearing loss by inhibiting MAPK and restoring the expression of PI3K [47].

Ras protein is a crucial signal regulator regulating the proliferation, differentiation, migration, and survival of different types of cells [48]. The Son of the sevenless (SOS)

family of Ras-GEF contains two widely expressed members (SOS1 and SOS2), which play a role in various signals in mammalian cells and promote Ras activation [49]. A prior analysis of conditional knockout mice showed that *Sos1* and *Sos2* play an essential role in homeostasis and overall organism survival [50]. *Sos1* depletion leads to specific phenotypic defects in MEFs, including alterations of mitochondrial morphology, mitochondrial dysfunctions, and metabolic defects [50–53]. Theard et al. [54] indicated that combined SOS1 and estimated glomerular filtration rate inhibition is an important target in estimated glomerular filtration rate-mutated lung adenocarcinoma. Recent studies showed that SOS activates membrane-tethered Ras and triggers MAPK cascade [55], while inhibition of the Grb2–Sos interaction downregulates Raf/MEK/ERK signaling [56]. The basic composition in MAPK cascades includes MAP3Ks, MAP2Ks, and MAPKs, which are highly conserved from yeast to humans. These three kinases are activated in turn, together regulating various physiological processes, including control of cellular proliferation, growth, differentiation, and inflammation [57]. MAP3K3, also known as MEKK3, belongs to the MAP3K superfamily. MAP3K3 is the key kinase of the MAPK signaling pathway and plays a crucial role in cell proliferation, apoptosis, and inflammatory and immune responses [58]. Previous studies showed that MAP3K3 plays a role in promoting cell survival, and MAP3K3 could promote mitochondrial degradation through the MAP3K3/MEK5/ERK5 pathway, thus increasing the content of mitochondria [59], while overexpression of *Map3k3* offers resistance to apoptosis via activating the nuclear factor κB signal pathway [60]. More recently, Yuan et al. determined that the *Map3k2/3* deficiency led to increased total ROS from neutrophils upon stimulation by fMLP, MIP2, or PMA, indicating the importance of kinase activity in the regulation of ROS release [61].

Our current H3K4me3-CUT&Tag-qPCR data revealed lower enrichment of H3K4me3 at the promoters of *Sos1* and *Sos2* and in *Map3k3* genes in CP-treated cells compared to control cells, suggesting that *Sos1*, *Sos2*, and *Map3k3* are epigenetic targets of KDM5A. However, the expression of these genes increased following the addition of CPI-455 to CP-treated cells, which is related to the increased occupation of H3K4me3 in the promoter region of these genes. Our study revealed that H3K4me3-dependent epigenetic activation of MAPK target genes was associated with HC survival, but the specific molecular mechanism in HC biology need further investigation. We still do not understand how CPI-455-mediated H3K4me3 is fully recognized, affecting other epigenetic modifications to regulate gene expression and inhibit HC apoptosis. Detailed CUT&Tag-seq analysis of CPI-455-mediated H3K4me3 and other histone marks would facilitate understanding their roles in transcriptional regulation. The mechanisms through which MAPK and PI3K/AKT modulate HC senescence have not been fully clarified. Epistasis between MAPK and PI3K/AKT can be further analyzed by in vivo pharmacogenetic intervention.

Despite the encouraging results reported here, this study still has some limitations. For example, KDM5A histone lysine demethylase inhibitor CPI-455 was reported to induce apoptosis and inhibit the proliferation of many tumor cells, such as cervical [62] and prostate cancer [63]. Our study observed synergistic effects between CPI-455 and CP in tumor suppression. Therefore, it is unlikely to interfere with the therapeutic effect of CP during tumor chemotherapy. Various KDM5A target genes were identified through a genome-wide study, which is necessary for mitochondrial function or DNA metabolism [21]. In tumor cells, by removing H3K4me3, KDM5A inhibits multiple tumor suppressor genes involved in the cell cycle [19], invasion [64], epithelial–mesenchymal transition [65], and other processes that contribute to tumor progression [66, 67]. CPI-455 treatment elevated global levels of H3K4me3 and reduced the number of drug-resistant persistent cancer cells in multiple tumor cell line models receiving antitumor drugs [34]. Based on the analysis and preliminary validation of mitochondrial function and multi-omics data, we concluded that CPI-455 is critical to ROS reduction and could improve mitochondrial function by activating Ras/MAPK and PI3K/AKT signaling, which is a fundamental mechanism for protecting HC from oxidative damage. In other words, KDM5A plays an important role in both normal tissue protection and tumor suppression and is, therefore, a promising target for CP-induced ototoxicity. Future work to gain more insights into the function of CPI-455 in chemosensitivity induced by CP is warranted, and the balance of KDM5A levels in ototoxic diseases also needs to be considered when developing KDM5A inhibition-based therapies. In addition, we confirmed the protective role of KDM5A inhibition in CP-induced SGN injury, although this may not fully reflect the situation in adult mice in vivo. In future work, we will evaluate the protective effect of CPI-455 on SGNs using CAP recording, which reflects the total cochlear nerve output from IHC to the auditory nerve.

Adeno-associated virus (AAV) is an effective vector for treating hearing loss. Many studies aim to restore hearing in mouse hearing loss models using AAV vectors. For example, Gu et al. demonstrated the protective effect of the AAV–CRISPR/Cas9–*Htra2* system against neomycin-induced ototoxicity in vitro [68]. However, in vivo, no significant protective effect was observed in cochlear basal OHCs due to the low transduction efficiency of Anc80L65 in OHCs [69, 70]. Iizuka et al. attempted to restore auditory function in *Gjb2* conditional knockout mice (P42) by delivering AAV5-*Gjb2* [71], and Pan et al. delivered AAV2/Anc80L65-*Ush1c* in Usher syndrome type 1c knock-in mice (P10–12) to restore the hearing [72]. However, both experiments failed

to rescue the auditory function of the treated mice, possibly due to low transduction efficiency or the closed therapeutic window. To further realize the clinical transformation of this treatment strategy based on AAV–CRISPR/cas9, in-depth research is needed to improve transfection efficiency, select the appropriate therapeutic window and surgical method, and evaluate the longer term safety profile. Our findings showed that inhibition of KDM5A led to an upregulated H3K4me3 level and the expression level of MAPK and PI3K/AKT target genes and promoted HC survival and hearing function after CP exposure both in vitro and in vivo. In future work, we will select the appropriate AAV–CRISPR/ Cas9 system and optimal surgical procedures to verify the role of KDM5A in hearing protection.

Conclusion

The present study showed that KDM5A participates in CP-induced hearing loss. KDM5A inhibition could protect against CP-induced ototoxicity, functioning via downregulation of oxidative stress, ROS production, and restoration of mitochondrial bioenergetic dysfunction. In addition, KDM5A inhibition reduces apoptosis by regulating a set of survival signaling pathways. Our findings have broad significance and call for the transformation of KDM5A as a potential therapeutic target for the treatment of hearing loss in the future.

Materials and methods

Compounds

CPI-455 (S8287; Selleckchem, Houston, TX, USA) was dissolved as 10 mmol/L of stock solution with DMSO (D5879; Sigma-Aldrich, St. Louis, MO, USA). CP was purchased from Sigma-Aldrich (479,306; Sigma-Aldrich) and was initially dissolved in PBS at a stock concentration of 3 mmol/L and further diluted in the medium used for cell and explant culture analysis.

Cell cultures

HEI-OC1 cells were cultured in high-glucose DMEM (11965-092; Gibco, Thermo Fisher Scientific, Inc., Waltham, MA, USA) supplemented with 10% FBS (10099-141; Gibco) at 33 °C under a 10% CO_2 condition [73–77]. FaDu and HGC-27 cell lines, preserved in our laboratory, were used before the 15th passage, and all experiments were performed in triplicate. Both cells were cultured in RPMI-1640 medium (C11875500BT; Gibco) containing 10% FBS and penicillin–streptomycin (15140-122; Gibco) under a

5% CO_2 condition. The cells were trypsinized with 0.25% trypsin/EDTA (25200056; Gibco) at 80% confluence.

Postnatal cochlear and SGN explants cultures and drug treatments

Animal experiments and research protocols were in accordance with the Fudan University Institutional Animal Care and Use Committee. Cochlea or SGNs explants from C57BL/6 mice at postnatal day 2 were dissected in PBS and attached to cell-Tak-coated coverslips. Then, explants were cultured in DMEM/F12 (C11330500BT; Gibco), containing 1% N2 (100 ×, 17502-048; Gibco) supplement, 2% B27 (50 ×, 17504-044; Gibco) supplement, and ampicillin (P0781; Sigma-Aldrich) at 37 °C and 5% CO_2.

In vivo study

Adult 8-week-old C57BL/6 mice were randomly divided into the following groups: control, CP, CPI-455, and CPI-455 + CP groups. 1 mg/mL CP stock solution was prepared in sterile saline (0.9% NaCl). The mice in the CP group received three rounds of once-daily intraperitoneal injections of CP at a dose of 3.5 mg/kg for 4 days, followed by a 10-day recovery period (a total of 42 days), as previously described [23, 78]. Mice in the CPI-455 + CP group received intraperitoneal injections of CPI-455 (0.5 mg/kg or 2 mg/ kg) starting 1 day before the injection of CP, and each cycle lasted for 5 days. Mice in the control and CPI-455 groups were injected with the same volume of saline or CPI-455, respectively.

For the high-dose CP-induced ototoxicity experiment, C57BL/6 mice were injected intraperitoneally with 1 mL of warm saline. After 24 h, CPI-455 was injected intraperitoneally 2 h in advance in mice of the CPI-455 + CP group and CPI-455 group; then, a single dose of CP (30 mg/kg) was injected intraperitoneally in mice of the CPI-455 + CP group and CP group. The ABR threshold was measured 14 days after administration.

ABR

ABR recording was implemented with the TDT system (Tucker Davis Technologies, Alachua, FL, USA). Mice were commonly anesthetized using a ketamine (100 mg/ kg)–xylazine (10 mg/kg) cocktail before measuring ABR. The recording, reference, and ground electrodes were inserted at the midpoint of the line joining the anterior edge of the auricle on each side, behind the tested ear, and behind the contralateral ear of the mouse. The SigGenRZ software (Tucker Davis Technologies) performed the ABR tests at 8-, 16-, 24-, and 32-kHz frequencies. The tone bursts were selected to evoke ABR, and the sound intensity was

attenuated gradually from 90 to 20 dB at intervals of 5 dB. The response for each frequency level was analyzed, digitized, and averaged using the BioSigRZ software (1024 samples/level). The amplitude of ABR wave I was determined by analyzing ABR waveforms.

ROS detection

ROS production was detected using CellROX™ green (C10444; Invitrogen, Carlsbad, CA, USA) and MitoSOX™ red (M36008; Invitrogen) according to the method described previously [79, 80]. For analyzing ROS levels in HEI-OC1 cells, cells were incubated with 5 μmol/L of CellROX™ green (excitation/emission maxima of 488/520 nm) working solution at 37 °C for 30 min in the dark. Then, HEI-OC1 cells were stained with 10 μg/mL Hoechst 33,258 (excitation/emission maxima of 350/461 nm) (861,405; Sigma–Aldrich) for 5 min, and the images were observed and captured with a confocal fluorescence microscope (Leica TCS SP8; Leica Microsystems GmbH, Wetzlar, Germany). Fluorescent signal intensity was taken with flow cytometry. Flow cytometric analysis used a Beckman Coulter MoFlo XDP (Miami, FL, USA) with FlowJo software (Version 10; TreeStar, Ashland, OR). CellROX™ fluorescence intensity was detected at an excitation wavelength of 488 nm and an emission wavelength of 520 nm (FL-1) by flow cytometry with gating at 20,000 cells/sample and the mean fluorescence intensity used to represent the amount of ROS. All experiments were repeated three times.

Regarding ROS assessment in the cochlea, cochlear explants from different treatments were incubated with 5 μmol/L of MitoSOX™ red (excitation/emission maxima of 510/580 nm) at 37 °C for 30 min in the dark. Fluorescent signal intensity was taken with fluorescence microscopy. Briefly, the representative images of the cochleae in each turn were randomly captured with a confocal fluorescence microscope under the same settings. MitoSOX™ red immunofluorescence was quantified by ImageJ software (National Institutes of Health, Bethesda, MD, USA) from raw confocal images that were taken under the same conditions at $63 \times$ magnification lens with a $0.75 \times$ digital zoom and with the same laser gain and PMT gain parameters. Cochlear explants were stained with a rabbit polyclonal antibody to Myosin 7a (1:500, 25–6790; Proteus Biosciences, Ramona, CA, USA) to determine comparable portions of the HCs in confocal images. Grayscale values were determined in the HCs to quantify changes in fluorescence intensity. The MitoSOX™ red signal was measured in the apical, middle, and basal turns of cochlear explant. The intensity of the background was subtracted and the mean intensity was then calculated. For each replicate, the relative fluorescence intensity values were determined by ratio normalization with the control group.

MMP measurement

MMP level was measured with Rhodamine 123 (C0062; LifeSct LLC, Rockville, USA) staining [79]. HEI-OC1 cells were incubated with 1 μmol/L of Rhodamine 123 at 37 °C for 30 min. Cells were then visualized under the same settings using a confocal fluorescence microscope.

For analyzing MMP levels in HEI-OC1 cells, cells were treated with trypsin, centrifuged at 1000 rpm for 5 min, and then rinsed twice with PBS. Next, HEI-OC1 cells were incubated in the dark with 1 μmol/L of Rhodamine 123 for 30 min at 37 °C, followed by flow cytometric analysis using the FACScan flow cytometer (Beckman Coulter) for a cell count of 20,000, and the data were analyzed using FlowJo software. Rhodamine 123 fluorescence intensity was detected at an excitation wavelength of 488 nm and an emission wavelength of 534 nm and the mean fluorescence intensity used to represent the levels of MMP. The experiments were repeated three times.

Apoptosis detection

For the TUNEL (terminal deoxynucleotidyl transferase-mediated dUTP nick-end labeling) (11684795910; Roche Holding, Basel, Switzerland) test, cochlear explants were washed with PBS for 15 min and then treated with the reaction mixture at 37 °C for 30 min. Myosin 7a and DAPI were used for HCs and nuclei counterstain, respectively. Representative images of each turn of the cochleae were captured randomly with a confocal fluorescence microscope under the same settings. The number of Myosin 7a/TUNEL-positive cells were counted in the images, and the results were averaged for three images per turn (apex, middle, and base) and expressed as data per 200 μm.

For the Annexin V conjugated to FITC (556547; BD Biosciences, San Jose, CA, USA) assay, HEI-OC1 cells were harvested and washed in PBS, then 2×10^5 cells were resuspended in a solution containing Annexin V (5 μL) and PI (5 μL) and incubated for 20 min. After incubation, 300 μL of binding buffer was added and the cells were analyzed by flow cytometry. All experiments were repeated three times. Cells with positive Annexin V-FITC staining and negative PI staining were considered to be undergoing early apoptosis, and cells with positive Annexin V-FITC and PI staining were considered to be undergoing late apoptosis.

Cell viability detection

CCK-8 kit (CK04; Dojindo Laboratories) was used to measure the viability of the cells. Briefly, HEI-OC1 cells were seeded in 96-well plates. After drug treatment, 10 μL of Cell Counting Kit-8 solution and 90 μL of culture medium were mixed, added to each well, and incubated for 3 h.

Absorbance was measured at 450 nm using a microplate reader (Bio-Rad Laboratories, Hercules, CA, USA).

Seahorse assay

For evaluating the energy metabolism, HEI-OC1 cells were seeded in 180 μL of DMEM containing 10% FBS on Seahorse XF96-cell culture microplates (Seahorse Bioscience, Billerica, MA, USA) at the density of 1.5×10^4 cells/well. Cells were washed with ~180 μL of XF assay medium before the assay, then cultured at 37 °C for 60 min. OCR was detected by the Seahorse XF96 instrument (Seahorse Bioscience) following the injections of mixtures in the Seahorse XF Cell Mito Stress Kit (Seahorse Bioscience). The following mixtures were added in proper order: first, oligomycin (complex V inhibitor; 25 μL in port A) at a concentration of 2 μmol/L; second, carbonyl cyanide 4-(trifluoromethoxy) phenylhydrazone (FCCP; 25 μL in port B) at the concentration of 0.5 mmol/L; and, finally, rotenone/antimycin A (25 μL) (inhibitors of complex I and III; in port C) at the concentration of 0.1 μmol/L/1 μmol/L. The XF Cell Mito Stress Test Report Generator software (version 2.6.0.31) was used to calculate and integrate the experiment data, and the results were obtained after triplicate repetition. OCR normalization was defined as total protein/well.

KDM5A-siRNA transfection

HEI-OC1 cells (1×10^3) were seeded in six-well plate and transfected with KDM5A-siRNA at a 50 nmol/L concentration with Lipo 3000 Transfection Reagent (L3000001; Invitrogen) for 24 h. The transfection efficiency of knockdown was detected by qRT-PCR. The following KDM5A-siRNA was used: (1) KDM5A siRNA-01, sense: 5′-GCACAAUCC UAUGACACUUGG-3′, antisense: 5′-CCAAGUGUCAUA GGAUUGUGC-3′. (2) KDM5A siRNA-02, sense: 5′-GCA AAUGAGACAACGGAAA-3′, antisense: 5′-UUUCCG UUGUCUCAUUUGC-3′.

Immunofluorescence

Samples fixed with 4% PFA were permeabilized with 1% PBST for 30 min. Afterward, we blocked with 10% donkey serum in PBST for 1 h, followed by incubation with the following primary antibodies: Myosin 7a rabbit polyclonal antibody (1:500, 25–6790; Proteus Biosciences, Ramona, CA, USA), Tuj-1 mouse (IgG2a) monoclonal antibody (1:1000, 801202; Biolegend, USA), parvalbumin mouse monoclonal antibody (1:1000, ab277625; Abcam, Cambridge, MA, USA), CtBP2 mouse (IgG1) monoclonal antibody (1:1000, 612044; BD Transduction Laboratories, BD Biosciences), GluR2 mouse (IgG2a) monoclonal antibody (1:1000, MAB397; Millipore Corp., Billerica, MA,

USA), H3K4me3 rabbit monoclonal antibody (1:500, 9751; Cell Signaling Technology, CST Danvers, MA, USA), and KDM5A rabbit monoclonal antibody (1:500, 3876; CST). Samples were then washed with PBS, followed by incubation with Alexa Fluor 488 donkey anti-rabbit/mouse or cy3-conjugated secondary antibody (1:1000, Invitrogen) along with DAPI (1:2000, D9542; Sigma-Aldrich) for 2 h. For image acquisition, all images were scanned with a laser scanning confocal fluorescence microscope (SP8; Leica) with a 40 × oil immersion objective lens as seen in Fig. 4A–C, or 63 × oil immersion objective lens as seen in Figs. 1A–C, 2A–C, 3A–C, 5D–F, 6A–C, 7C–D, 8D, G, and S1D–F under identical z-stack conditions (in 1 μm Z-steps) and the same laser intensity, gains, and PMT gains parameter settings.

H&E staining

After mice were sacrificed, their hearts, livers, spleens, and lungs were harvested for H&E staining. The sections were deparaffinized twice with xylene (for 20 min each), then rehydrated twice with 100% alcohol (for 5 min each), then rehydrated with 75% alcohol (for 5 min each) and rinsed with water. The sections were stained with Harris hematoxylin solution, counterstained with eosin solution, then dehydrated three times in 100% alcohol (5 min each), and washed twice with xylene (5 min each). Finally, these sections were observed under a light microscope.

Western blot analysis

Protein lysate from cells and cochlear sensory epithelia for each group was prepared in RIPA buffer (P0013B; Beyotime Biotech) with the addition of protease inhibitor (04693132001; Sigma-Aldrich), followed by placement on ice for 30 min, being shaken every 10 min. After the centrifugation at 12,000 rpm at 4 °C for 10 min, the supernatants were denatured and loaded on 12% SDS-PAGE gel. Proteins were then transferred in an ice bath to polyvinylidene difluoride membrane (Immobilon-P, IPVH00010; Millipore, Schaffhausen, Switzerland). After blocking with TBST buffer containing 5% milk for 1 h, the membrane was incubated with primary antibodies overnight at 4 °C, followed by secondary antibody. The antibodies were as follows: cleaved caspase-3 rabbit polyclonal antibody (1:500, 9661; CST), caspase-3 rabbit polyclonal antibody (1:500, 9662; CST), Bax rabbit monoclonal antibody (1:500, 14,796; CST), Bcl-2 rabbit monoclonal antibody (1:500, 3498; CST), phospho-Akt (Ser473) rabbit monoclonal antibody (1:500, 4060; CST), Akt rabbit monoclonal antibody (1:500, 4691; CST), phospho-PI3K rabbit monoclonal antibody (1:500, 17,366; CST), PI3K rabbit monoclonal antibody (1:500, 4257; CST), phospho-p38

MAPK (Thr180/Tyr182) rabbit monoclonal antibody (1:500, 4511; CST), p38 MAPK rabbit polyclonal antibody (1:500, 9212; CST), phospho-JNK rabbit monoclonal antibody (1:1,000, ab124956; Abcam), JNK rabbit monoclonal antibody (1:1,000, ab179461; Abcam), KDM5A rabbit monoclonal antibody (1:500, 3876; CST), KDM5B rabbit polyclonal antibody (1:500, 3273; CST), KDM5C rabbit monoclonal antibody (1:500, 5361; CST), H3K4me3 rabbit monoclonal antibody (1:500, 9751; CST), horseradish peroxidase-linked donkey anti-rabbit IgG polyclonal antibody (1:3,000, 406,401; Biolegend, San Diego, CA, USA), and goat anti-mouse IgG polyclonal antibody (1:3,000, GTX213111-01; GeneTex, Irvine, CA, USA). Each experiment was repeated three times, and GAPDH mouse monoclonal antibody (1:1,000, 437,000; Invitrogen) was used as an internal reference protein. Finally, signals were detected by GE Healthcare's ECL detection reagent (GE Healthcare, Chicago, IL, USA).

RNA-Seq and real-time RT-PCR

Total RNA integrity was assessed using an Agilent 2100 biological analyzer (Agilent Technologies, Santa Clara, CA, USA). Samples with RNA integrity values of > 7.0 were used for RNA-Seq. The complementary DNA libraries were sequenced on the Illumina HiSeq X Ten platform. The differential expression was analyzed using the software DESeq (2012) R package. $P < 0.05$, fold-change > 2, and FDR < 0.01 were set as the thresholds for significant differential expression. Based on the hypergeometric distribution, R was used to enrich differentially expressed genes by Gene Ontology and KEGG, respectively. For quantification of gene expression, the $2^{-\Delta\Delta CT}$ method was used and normalized against GAPDH expression. The primers of all primer sets used in these experiments are shown in Online Table 1.

CUT&Tag

CUT&Tag for bench-top application was performed using 100,000 cells as previously published [81]. More detailed information can be found at the website: http://protocols.io/view/bench-top-cut-amp-tag-wnufdew/abstract. The primary antibody was H3K4me3 rabbit monoclonal antibody (1:500, 9751; CST), and the secondary antibody was goat anti-rabbit IgG (AS070; ABclonal, Wuhan, China). The DNAs were extracted and subjected to PCR. The primers of all primer sets used in these experiments are shown in Online Table 1. The experiments were repeated three times independently and the results were normalized to the IgG control.

HC, SGN, and synapse counts

Quantification of HCs, SGNs, and synapses was performed in the apical, middle, and basal turns of the cochlea. For the evaluation of HC, we took $63 \times$ magnified confocal images of each turn of the cochlea at random as representative images. We calculated the number of total HCs in the images, averaged the results for three images from each turn, and presented the data as per 200 μm. For cultured SGN explants, the fluorescence images were acquired using confocal laser microscopy with a $40 \times$ oil immersion objective with a $0.75 \times$ digital zoom and a 1 μm step size between each plane. The length of SGN neurites and the SGN density per 100 μm were calculated. For synaptic quantification, we obtained confocal z-stacks images of IHC area from each turn with a $63 \times$ oil immersion objective with a $2 \times$ digital zoom and a 1 μm step size between each plane. Z-stacks were allowed to span all IHCs, including all synaptic ribbons. We imported the image stacks into ImageJ (National Institutes of Health, Bethesda, MD, USA) and then manually calculated the CtBP2 or GluR2 puncta in each image stack. The number of CtBP2 or GluR2 puncta per IHC within a 100 μm range was calculated in three different regions of every turn of the cochlea.

Statistical analyses

Data were analyzed and plotted by GraphPad Prism software (San Diego, CA, USA) and shown as mean $\pm$ SEM. Quantitative data statistical analysis was assessed using one-way analysis of variance (ANOVA) for multiple group comparisons or two-tailed Student's t tests for two-group data. $P < 0.05$ was considered as significant.

Declarations

Conflict of interest The authors declare that they have no competing interests.

Ethics approval and consent to participate No human data or tissue were involved. All animal research protocols were approved by the Institutional Animal Care and Use Committee of Fudan University.

Consent for publication Not applicable.

References

1. Cepeda V, Fuertes MA, Castilla J, Alonso C, Quevedo C, Perez JM (2007) Biochemical mechanisms of cisplatin cytotoxicity. Anti-Cancer Agent Me 7:3–18

2. Rybak LP, Whitworth CA, Mukherjea D, Rarakumar V (2007) Mechanisms of cisplatin-induced ototoxicity and prevention. Hearing Res 226:157–167

3. Kim KH, Lee B, Kim YR et al (2018) Evaluating protective and therapeutic effects of alpha-lipoic acid on cisplatin-induced ototoxicity. Cell Death Dis 9:8

4. Landier W (2016) Ototoxicity and cancer therapy. Cancer 122:1647–1658

5. Wang W, Wu KJ, Vellaisamy K, Leung CH, Ma DL (2020) Peptide-conjugated long-lived theranostic imaging for targeting GRPr in cancer and immune cells. Angew Chem Int Ed Engl 59:17897–17902

6. Nickols NG, Jacobs CS, Farkas ME, Dervan PB (2007) Modulating hypoxia-inducible transcription by disrupting the HIF-1-DNA interface. Acs Chem Biol 2:561–571

7. Ma L, Li GX, Zhu HQ et al (2014) 2-Methoxyestradiol synergizes with sorafenib to suppress hepatocellular carcinoma by simultaneously dysregulating hypoxia-inducible factor-1 and-2. Cancer Lett 355:96–105

8. Kiefer RM, Hunt SJ, Pulido S et al (2017) Relative initial weight is associated with improved survival without altering tumor latency in a translational rat model of diethylnitrosamine-induced hepatocellular carcinoma and transarterial embolization. J Vasc Interv Radiol 28:1043–1050

9. Bo R, Yasen A, Shao YM et al (2020) Co-existence of hepatocellular carcinoma and cystic echinococcosis. Infect Agents Cancer 15:1

10. Kang BS, Lee SE, Ng CL, Kim JK, Park JS (2015) Exploring the preparation of albendazole-loaded chitosan-tripolyphosphate nanoparticles. Materials 8:486–498

11. Li A, He YZ, Sun S, Cai CF, Li HW (2015) Lysine-specific demethylase 1 inhibitors protect cochlear spiral ganglion neurons against cisplatin-induced damage. NeuroReport 26:539–547

12. He YZ, Yu HQ, Cai CF, Sun S, Chai RJ, Li HW (2015) Inhibition of H3K4me2 demethylation protects auditory hair cells from neomycin-induced apoptosis. Mol Neurobiol 52:196–205

13. Li A, You D, Li W et al (2018) Novel compounds protect auditory hair cells against gentamycin-induced apoptosis by maintaining the expression level of H3K4me2. Drug Deliv 25:1033–1043

14. He YZ, Li W, Zheng ZW et al (2020) Inhibition of protein arginine methyltransferase 6 reduces reactive oxygen species production and attenuates aminoglycoside- and cisplatin-induced hair cell death. Theranostics 10:133–150

15. Yu H, Lin Q, Wang Y et al (2013) Inhibition of H3K9 methyltransferases G9a/GLP prevents ototoxicity and ongoing hair cell death. Cell Death Dis 4:e506

16. Collins BE, Greer CB, Coleman BC, Sweatt JD (2019) Histone H3 lysine K4 methylation and its role in learning and memory. Epigenet Chromatin 12:1

17. Klose RJ, Yan Q, Tothova Z et al (2007) The retinoblastoma binding protein RBP2 is an H3K4 demethylase. Cell 128:889–900

18. Varaljai R, Islam ABMMK, Beshiri ML, Rehman J, Lopez-Bigas N, Benevolenskaya EV (2015) Increased mitochondrial function downstream from KDM5A histone demethylase rescues differentiation in pRB-deficient cells. Gene Dev 29:1817–1834

19. Beshiri ML, Holmes KB, Richter WF et al (2012) Coordinated repression of cell cycle genes by KDM5A and E2F4 during differentiation. Proc Natl Acad Sci USA 109:18499–18504

20. Chicas A, Kapoor A, Wang XW et al (2012) H3K4 demethylation by Jarid1a and Jarid1b contributes to retinoblastoma-mediated gene silencing during cellular senescence. Proc Natl Acad Sci USA 109:8971–8976

21. Lopez-Bigas N, Kisiel TA, DeWaal DC et al (2008) Genome-wide analysis of the H3K4 histone demethylase RBP2 reveals a transcriptional program controlling differentiation. Mol Cell 31:520–530

22. Plch J, Hrabeta J, Eckschlager T (2019) KDM5 demethylases and their role in cancer cell chemoresistance. Int J Cancer 144:221–231

23. Liang Z, Zhang T, Zhan T et al (2021) Metformin alleviates cisplatin-induced ototoxicity by autophagy induction possibly via the AMPK/FOXO3a pathway. J Neurophysiol 125:1202–1212

24. Liu K, Jiang X, Shi C et al (2013) Cochlear inner hair cell ribbon synapse is the primary target of ototoxic aminoglycoside stimuli. Mol Neurobiol 48:647–654

25. Tabuchi K, Nishimura B, Nakamagoe M, Hayashi K, Nakayama M, Hara A (2011) Ototoxicity: mechanisms of cochlear impairment and its prevention. Curr Med Chem 18:4866–4871

26. Mignotte B, Vayssiere JL (1998) Mitochondria and apoptosis. Eur J Biochem 252:1–15

27. Zeng JP, Ge Z, Wang LX et al (2010) The histone demethylase RBP2 is overexpressed in gastric cancer and its inhibition triggers senescence of cancer cells. Gastroenterology 138:981–992

28. Lin WC, Cao J, Liu JY et al (2011) Loss of the retinoblastoma binding protein 2 (RBP2) histone demethylase suppresses tumorigenesis in mice lacking Rb1 or Men1. Proc Natl Acad Sci USA 108:13379–13386

29. Hou JL, Wu J, Dombkowski A et al (2012) Genomic amplification and a role in drug-resistance for the KDM5A histone demethylase in breast cancer. Am J Transl Res 4:247–256

30. Cao J, Liu ZZ, Cheung WKC et al (2014) Histone demethylase RBP2 is critical for breast cancer progression and metastasis. Cell Rep 6:868–877

31. Teng YC, Lee CF, Li YS et al (2013) Histone demethylase RBP2 promotes lung tumorigenesis and cancer metastasis. Can Res 73:4711–4721

32. Kong SY, Kim W, Lee HR, Kim HJ (2018) The histone demethylase KDM5A is required for the repression of astrocytogenesis

and regulated by the translational machinery in neural progenitor cells. FASEB J 32:1108–1119

33. Liu Y, Yu YM, Zhang JC, Wang CT (2019) The therapeutic effect of dexmedetomidine on protection from renal failure via inhibiting KDM5A in lipopolysaccharide-induced sepsis of mice. Life Sci 239:116868

34. Vinogradova M, Gehling VS, Gustafson A et al (2016) An inhibitor of KDM5 demethylases reduces survival of drug-tolerant cancer cells. Nat Chem Biol 12:531–538

35. Spongr VP, Flood DG, Frisina RD, Salvi RJ (1997) Quantitative measures of hair cell loss in CBA and C57BL/6 mice throughout their life spans. J Acoust Soc Am 101:3546–3553

36. Willott JF (2009) Effects of sex, gonadal hormones, and augmented acoustic environments on sensorineural hearing loss and the central auditory system: insights from research on C57BL/6J mice. Hear Res 252:89–99

37. Park SN, Back SA, Park KH et al (2010) Comparison of cochlear morphology and apoptosis in mouse models of presbycusis. Clin Exp Otorhinolaryngol 3:126–135

38. Zhang C, Sun W, Li J et al (2017) Loss of sestrin 2 potentiates the early onset of age-related sensory cell degeneration in the cochlea. Neuroscience 361:179–191

39. Kane KL, Longo-Guess CM, Gagnon LH, Ding D, Salvi RJ, Johnson KR (2012) Genetic background effects on age-related hearing loss associated with Cdh23 variants in mice. Hear Res 283:80–88

40. White JA, Burgess BJ, Hall RD, Nadol JB (2000) Pattern of degeneration of the spiral ganglion cell and its processes in the C57BL/6J mouse. Hear Res 141:12–18

41. Xiong W, Yu S, Liu K, Gong S (2020) Loss of cochlear ribbon synapses in the early stage of aging causes initial hearing impairment. Am J Transl Res 12:7354–7366

42. Jiang XW, Li XR, Zhang YP (2015) Changes of ribbon synapses number of cochlear hair cells in C57BL/6J mice with age(Delta). Int J Clin Exp Med 8:19058–19064

43. Zhang R, Chae S, Lee JH, Hyun JW (2012) The cytoprotective effect of butin against oxidative stress is mediated by the up-regulation of manganese superoxide dismutase expression through a PI3K/Akt/Nrf2-dependent pathway. J Cell Biochem 113:1987–1997

44. Aburto MR, Magarinos M, Leon Y, Varela-Nieto I, Sanchez-Calderon H (2012) AKT signaling mediates IGF-I survival actions on otic neural progenitors. PLoS ONE 7:e30790

45. Dinh CT, Goncalves S, Bas E, Van De Water TR, Zine A (2015) Molecular regulation of auditory hair cell death and approaches to protect sensory receptor cells and/or stimulate repair following acoustic trauma. Front Cell Neurosci 9:96

46. Van Rossom S, de Beeck KO, Hristovska V, Winderckx J, Van Camp G (2015) The deafness gene DFNA5 induces programmed cell death through mitochondria and MAPK-related pathways. Front Cell Neurosci 9

47. Zhang Y, Huang S, Dai X et al (2021) SOD2 alleviates hearing loss induced by noise and kanamycin in mitochondrial DNA4834-deficient rats by regulating PI3K/MAPK signaling. Curr Med Sci 41:587–596

48. Fernandez-Medarde A, Santos E (2011) Ras in cancer and developmental diseases. Genes Cancer 2:344–358

49. Baltanas FC, Zarich N, Rojas-Cabaneros JM, Santos E (2020) SOS GEFs in health and disease. Biochim Biophys Acta Rev Cancer 1874:188445

50. Baltanas FC, Perez-Andres M, Ginel-Picardo A et al (2013) Functional redundancy of Sos1 and Sos2 for lymphopoiesis and organismal homeostasis and survival. Mol Cell Biol 33:4562–4578

51. Garcia-Navas R, Liceras-Boillos P, Gomez C et al (2021) Critical requirement of SOS1 RAS-GEF function for mitochondrial dynamics, metabolism, and redox homeostasis. Oncogene 40:4538–4551

52. Liceras-Boillos P, Garcia-Navas R, Ginel-Picardo A et al (2016) Sos1 disruption impairs cellular proliferation and viability through an increase in mitochondrial oxidative stress in primary MEFs. Oncogene 35:6389–6402

53. Suire S, Baltanas FC, Segonds-Pichon A et al (2019) Frontline science: TNF-alpha and GM-CSF1 priming augments the role of SOS1/2 in driving activation of Ras, PI3K-gamma, and neutrophil proinflammatory responses. J Leukoc Biol 106:815–822

54. Theard PL, Sheffels E, Sealover NE, Linke AJ, Pratico DJ, Kortum RL (2020) Marked synergy by vertical inhibition of EGFR signaling in NSCLC spheroids shows SOS1 is a therapeutic target in EGFR-mutated cancer. Elife 9.

55. Mor A, Philips MR (2006) Compartmentalized Ras/MAPK signaling. Annu Rev Immunol 24:771–800

56. Holt KH, Waters SB, Okada S et al (1996) Epidermal growth factor receptor targeting prevents uncoupling of the Grb2-SOS complex. J Biol Chem 271:8300–8306

57. Group M (2002) Mitogen-activated protein kinase cascades in plants: a new nomenclature. Trends Plant Sci 7:301–308

58. Fisher OS, Deng HQ, Liu D et al (2015) Structure and vascular function of MEKK3-cerebral cavernous malformations 2 complex. Nat Commun 6

59. Craig JE, Miller JN, Rayavarapu RR et al (2020) MEKK3-MEK5-ERK5 signaling promotes mitochondrial degradation. Cell Death Discov 6:107

60. Samanta AK, Huang HJ, Bast RC Jr, Liao WS (2004) Overexpression of MEKK3 confers resistance to apoptosis through activation of NFkappaB. J Biol Chem 279:7576–7583

61. Yuan QY, Basit A, Liang WH et al (2021) Pazopanib ameliorates acute lung injuries via inhibition of MAP3K2 and MAP3K3. Sci Transl Med 13

62. Zhang Y, Li X, Zhang J, Mao L (2020) E6 hijacks KDM5C/lnc_000231/miR-497-5p/CCNE1 axis to promote cervical cancer progression. J Cell Mol Med 24:11422–11433

63. Hong Z, Wu G, Xiang ZD et al (2019) KDM5C is transcriptionally regulated by BRD4 and promotes castration-resistance prostate cancer cell proliferation by repressing PTEN. Biomed Pharmacother 114:108793

64. Dai B, Huang H, Guan F et al (2018) Histone demethylase KDM5A inhibits glioma cells migration and invasion by down regulating ZEB1. Biomed Pharmacother 99:72–80

65. Feng T, Wang Y, Lang Y, Zhang Y (2017) KDM5A promotes proliferation and EMT in ovarian cancer and closely correlates with PTX resistance. Mol Med Rep 16:3573–3580

66. Yang GJ, Zhu MH, Lu XJ et al (2021) The emerging role of KDM5A in human cancer. J Hematol Oncol 14

67. Yang GJ, Wu J, Miao L et al (2021) Pharmacological inhibition of KDM5A for cancer treatment. Eur J Med Chem 226:113855

68. Gu X, Wang DQ, Xu ZJ et al (2021) Prevention of acquired sensorineural hearing loss in mice by in vivo Htra2 gene editing. Genome Biol 22:1

69. Suzuki J, Hashimoto K, Xiao R, Vandenberghe LH, Liberman MC (2017) Cochlear gene therapy with ancestral AAV in adult mice: complete transduction of inner hair cells without cochlear dysfunction (vol 7, 45524, 2017). Sci Rep-Uk 7

70. Isgrig K, McDougald D, Zhu J, Wang H, Bennett J, Chien W (2019) AAV2.7m8 is a powerful viral vector for inner ear gene therapy. Hum Gene Ther 30:A111–A111

71. Iizuka T, Kamiya K, Gotoh S et al (2015) Perinatal Gjb2 gene transfer rescues hearing in a mouse model of hereditary deafness. Hum Mol Genet 24:3651–3661

72. Pan B, Askew C, Galvin A et al (2017) Gene therapy restores auditory and vestibular function in a mouse model of Usher syndrome type 1c. Nat Biotechnol 35:264–272

73. Kalinec GM, Webster P, Lim DJ, Kalinec F (2003) A cochlear cell line as an in vitro system for drug ototoxicity screening. Audiol Neuro-Otol 8:177–189

74. He ZH, Sun S, Waqas M et al (2016) Reduced TRMU expression increases the sensitivity of hair-cell-like HEI-OC-1 cells to neomycin damage in vitro. Sci Rep-Uk 6

75. Kalinec G, Thein P, Park C, Kalinec F (2016) HEI-OC1 cells as a model for investigating drug cytotoxicity. Hear Res 335:105–117

76. Yang QQ, Zhou YW, Yin HY et al (2018) PINK1 protects against gentamicin-induced sensory hair cell damage: possible relation to induction of autophagy and inhibition of p53 signal pathway. Front Mol Neurosci 11

77. Zhou MJ, Sun GY, Zhang LL et al (2018) STK33 alleviates gentamicin-induced ototoxicity in cochlear hair cells and House Ear Institute-Organ of Corti 1 cells. J Cell Mol Med 22:5286–5299

78. Breglio AM, Rusheen AE, Shide ED et al (2017) Cisplatin is retained in the cochlea indefinitely following chemotherapy. Nat Commun 8

79. He Y, Zheng Z, Liu C et al (2022) Inhibiting DNA methylation alleviates cisplatin-induced hearing loss by decreasing oxidative stress-induced mitochondria-dependent apoptosis via the LRP1-PI3K/AKT pathway. Acta Pharm Sin B 12:1305–1321

80. Zheng S, Liu C, Tang D et al (2022) The protective effect of rutin against the cisplatin-induced cochlear damage in vitro. Neurotoxicology 90:102–111

81. Kaya-Okur HS, Wu SJ, Codomo CA et al (2019) CUT&Tag for efficient epigenomic profiling of small samples and single cells. Nat Commun 10:102

Publisher's Note Springer Nature remains neutral with regard to jurisdictional claims in published maps and institutional affiliations.